Contact No. - NAS9 - 13696
DRL NO. - MA - 183TA
Line Item No. - 4
Report No. - ATL-CR-75-04
NASA CR-
141665

Application of Acoustic Surface Wave Technology to Shuttle Radar

Final Report
January 1975

Prepared for:

LYNDON B. JOHNSON SPACE CENTER

NATIONAL AERONAUTICS AND SPACE ADMINISTRATION

HOUSTON, TEXAS 77058

Submitted by:

ADVANCED TECHNOLOGY LABORATORIES

RCA|GOVERNMENT AND COMMERCIAL SYSTEMS

CAMDEN, NEW JERSEY 08102

Application of Acoustic Surface Wave Technology to Shuttle Radar

Final Report
January 1975

Contract No. - NAS9 - 13696
DRL No. - MA - 183TA
Line Item No. - 4
Report No. - ATL-CR-75-04

Submitted by:

ADVANCED TECHNOLOGY LABORATORIES

RCA|GOVERNMENT AND COMMERCIAL SYSTEMS

CAMDEN, NEW JERSEY 08102

NASA Technical Monitor: _____
Ronald C. Kelly

ABSTRACT

The objective of this program was to explore the application of surface acoustic wave (SAW) signal processing devices in the Space Shuttle. The use of these devices in the rendezvous radar, instrument landing system, and radar altimeter was examined and discussed in a previous study report. In order to demonstrate the functions which SAW device might perform, a breadboard pulse compression filter (PCF) module was assembled. The PCF which is the subject of this report permits a pulse radar to operate with a large duty cycle and low peak power—a regime favorable to the use of solid state RF sources. This report describes the transducer design, strong coupling compensation, circuit model analysis, fabrication limitations, and performance evaluation of a PCF. The nominal value of the compression ratio is 100:1 with 10-MHz bandwidth centered at 60 MHz and 10-μs dispersive delay. The PCF incorporates dispersive interdigital transducers and a piezoelectric lithium niobate substrate.

FOREWORD

This final report is submitted under contract NAS9-13696 from the National Aeronautics and Space Administration, Lyndon B. Johnson Space Center, Houston, Texas. Ronald C. Kelly is the NASA Technical Monitor. The report was written by Mr. Dale Stepps of the RCA Advanced Technology Laboratories.

The author acknowledges the valuable assistance of Mr. H. Veloric and Mr. F. Wozniak for device fabrication, Mr. H. Hook, Mr. F. McFarland, Mr. D. Tamutus and Mr. W. Geshner for photomask production, and Mr. S. Perlman for the use of his filter design programs.

TABLE OF CONTENTS

DEFINITIONS

Apodization - variation of the finger overlap throughout the transducer to produce a desired frequency response.

Coupling Coefficient (k^2) - a figure of merit for acoustical-mechanical coupling between the surface and the electrode.

Dummy Fingers - inactive fingers used to maintain a linear phase front.

Interdigital Transducer (IDT) - a comb-like array of parallel fingers of alternating polarity with a specified overlap.

Matched Filter - conjugate filter used to compress an expanded FM pulse in the receiver.

Surface Acoustic Wave (SAW) - a Rayleigh wave that propagates on the surface of an piezoelectric elastic medium, e.g., quartz, lithium niobate.

Least Count (Step) - this number specifies the smallest increment of distance the artwork machine can move. The accuracy of the generator indicates how close to the least step the generator actually moves.

SUMMARY AND RESULTS

The design of a dispersive filter is discussed in detail covering the various compensation schemes for high coupling materials to adjust for changes in velocity with various stripe-to-gap ratios, acoustic reflections, wave diffraction, and Fresnel ripple. Two design approaches are presented with one utilizing a single dispersive geometry and the other a double dispersive geometry. Electrical characterization of the filter predicted 13-dB CW insertion loss with a radiation resistance of 4 ohms. The actual measured insertion loss was 10 dB at center frequency.

The matched filter was an exact duplicate of the expansion device incorporating internal weighting to suppress the time sidelobe levels. Three schemes to reduce the time sidelobes are presented. One utilizes an internal Hamming function to weight the output transducer of the matched filter. Another approach uses an external SAW Hamming filter to reduce sidelobes by frequency domain weighting. The last approach uses a weighted transmitted pulse into an internally weighted receiver.

The transmitter and receiver components were constructed on a single connective circuit board for simple operation and maintenance. A specially milled package houses both expansion and compression filters to maintain temperature tracking, to suppress RF feedthrough to below -35 dB, and to shield internally mounted amplifiers. The external SAW filter was mounted in an IC package.

CONCLUSIONS

This project has demonstrated that pulse compression can be implemented with SAW technology producing light-weight devices compatible with an all solid state radar system. The various approaches used in this project showed that both internal and external weighting methods reduced sidelobe levels to extend the dynamic range of the radar. Predictable insertion loss and weighting functions were accurately approximated with the interdigital transducer to perform the complex signal processing for pulse compression. Also, the pulse compression module used inexpensive, miniaturized devices to interface with the SAW filters on a single connective circuit board with low loss and adequate channel isolation.

The main problem encountered in this contract involved the production of photomasks with the necessary line spacing accuracy. The Gerber artwork generators and photo-reduction techniques available required a stepwise linear FM approximation with 20 frequency steps over a 10-MHz bandwidth. This resulted in an average cluster of 15 finger pairs per frequency step. Also, artwork generation limitations produced a frequency-time mismatch, reducing the active fingers by 15% in the compression mode.

All these factors inhibited the achievement of theoretical performance predictions of -30 dB sidelobe level. The result was a -18 dB sidelobe level with internal weighting and a rectangular transmitted pulse; the use of a weighted transmitted pulse, however, produced -27 dB sidelobes.

The high coupling coefficient of $LiBNO_3$ produced a severe triple transit response on the external weighting filter at 12.5 dB below the peak. This would prove to be undesirable in a radar system. The same filter design on ST quartz would have suppressed the triple transit response to below -40 dB. The 2-MHz center frequency mismatch between the compressed pulse and the external weighting filter limited the sidelobe suppression to an additional 2 dB to 20 dB below the peak.

In conclusion, the achievements obtained in this contract are useful in defining the necessary technology to produce a high performance pulse compression system. The first requirement is to utilize a photomask generation process that can achieve a .3-microinch least-step accuracy. All fabrication requirements such as line width and film thickness should be held within a 10% tolerance to reduce phase and velocity error accumulation.

INTRODUCTION

The goal of this program was to assemble and evaluate a dispersive filter with a pulse compression ratio of 100:1. The performance goals are shown in Table I.

TABLE I - DESIGN GOALS

1.	Compression Ratio	100:1
2.	Time Sidelobe Level	-30 dB
3.	Maximum compressed pulse width @ -4 dB point	200 ns
4.	Amplitude Ripple	±1 dB
5.	Insertion Loss @ Center Frequency	< 25 dB
6.	Center Frequency	60 MHz
7.	Bandwidth	10 MHz
8.	Phase Error	5° pp.

The second section of this report reviews the required backup electronics. The circuitry shapes the pulse for transmission and reception by performing functions such as frequency inversion, gating, amplification, and limiting. This section also describes temperature tracking and the packaging approach for both the transmitter and receiver. The performance of these components is also evaluated in the second section.

The third section discusses the design and analysis of the dispersive lines for pulse expansion. First, the important material parameters are outlined with a summary of the available materials for surface wave devices. Next, the basic IDT is presented and analyzed along with compensation for stripe-to-gap variance on the strong coupling material. Diffraction and apodization considerations are then discussed.

Section four describes the matched filter concept with the various approaches for obtaining sidelobe suppression. In this section the fabrication process and artwork generation problems are covered in detail.

This section also discusses the problems encountered with generation and fabrication of photomasks. Such problems reduce the Hamming function's ability to suppress time sidelobes. Also, mask fabrication problems led to the selection of a single photomask to generate and compress the FM signal.

PULSE COMPRESSION MODULE

Table II summarizes the pulse compression system operating parameters.

TRANSMITTER

Although the matched filters perform the actual pulse compression, the backup electronics shape the pulse for transmission and reception. (See Fig. 1). Signal processing in the transmitter section (Fig. 1a) entails inverting the frequency spectrum in time from a "down chirp" (high to low frequencies) to an "up chirp" (low to high frequencies) sweep, gating the pulse to 10 μs, then limiting the amplitude ripple to 1 dB. The FM signal is generated by impulsing the surface wave expander with a video pulse which contains enough RF content to provide a full FM burst. After the burst is generated, it mixes with a stable 120-MHz local oscillator to spectrally invert the signal in time (Fig. 2a). Next, a 3-pole Butterworth passive filter filters out the sum product. The pulse is then gated with a 50-mV 10-μs pulse to shape the pulse ends to the required time delay while limiting the pulse amplitude ripple (Fig. 2b.) Finally, a power splitter divides and isolates the pulse for monitor and transmit outputs. This completes the signal processing in the transmitter section, thus providing an inverted, rectangular, linear FM pulse ready for transmission and compression.

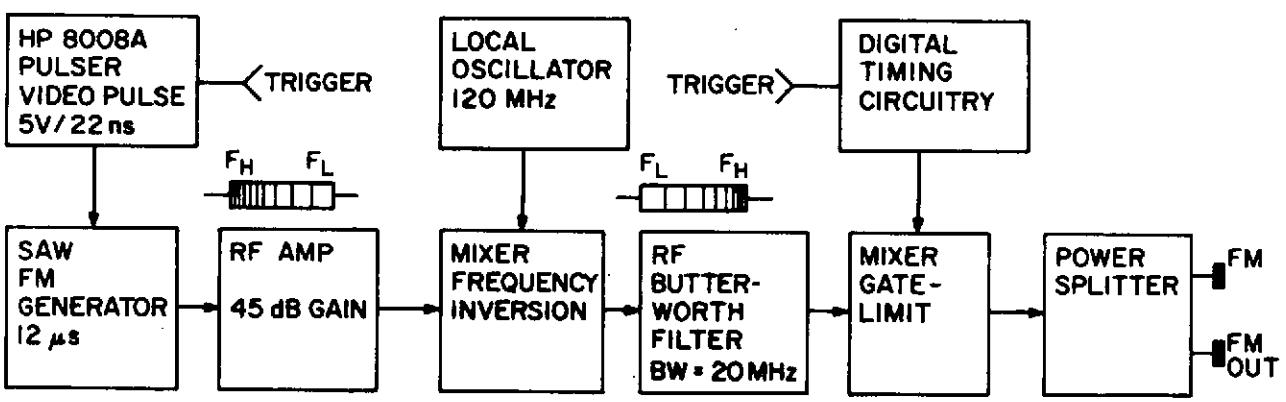

a) Transmitter.

b) Receiver.

Fig. 1. Transmitter and receiver block diagrams.

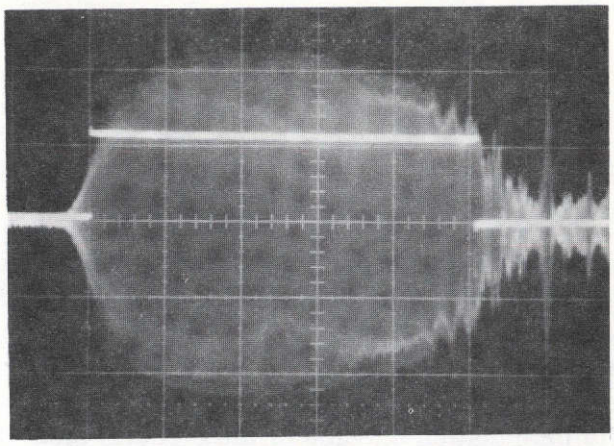

2 μs/div

Fig. 2a. Spectrally inverted FM burst with gate-limiting pulse.

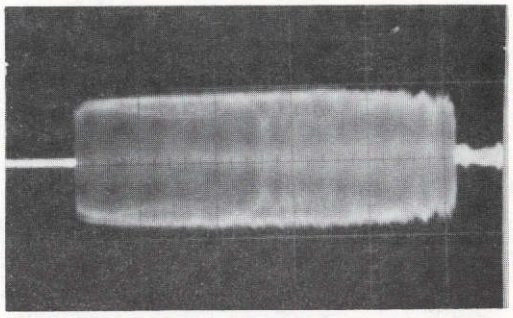

2 μs/div

Fig. 2b. Gated and limited FM burst.

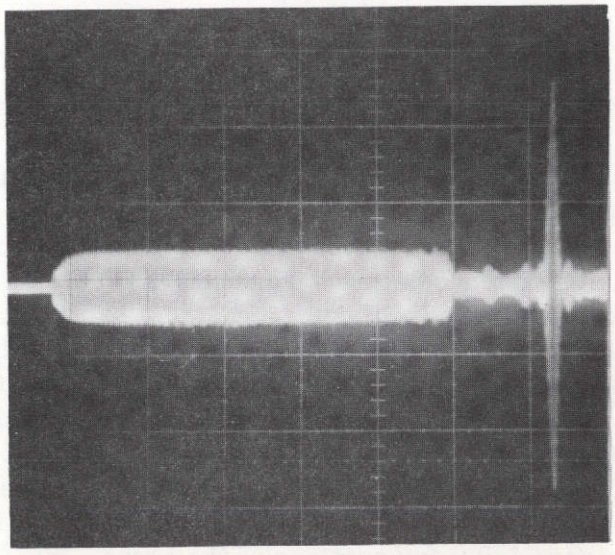

2 μs/div

Fig. 2c. Transmitter and receiver outputs together.

RECEIVER

The receiver, diagrammed in Fig. 1b, consists of a simple matched filter with an external weighting filter for sidelobe reduction to -30 dB below the main lobe peak, with appropriate amplification to offset the insertion loss of the devices. The actual received and compressed pulse after weighting are shown in Fig. 2c. This completes the basic steps taken in the prototype pulse compression system. However, subsequent sections provide specific information on each of the circuits mentioned above. Table II summarizes the operating parameters for both the transmitter and receiver.

TEMPERATURE CONSIDERATIONS

Since matched filters must maintain conjugate relationships through changing conditions, the separate expansion and compression filters were co-located in a single RF package to maintain temperature tracking (Fig. 3b). The package design also incorporated RF feedthrough suppression by isolating input and output connections, and reduced space requirements by providing amplification within the package.

Since the pulse centers at a relatively low frequency, a single connective printed circuit board was used which requires minimum space and provides low noise operation for both the transmitter and receiver. Figs. 3a, b and c show the board with components mounted in the final package. All outputs and inputs are BNC, while power connections are made using a special Deutsch 6823 hermetically sealed connector.

TIMING CIRCUIT DESCRIPTION

In Figs. 4a and b, the gate/limit circuit is formed by two series monostable multivibrators to provide a stable, completely adjustable, limiting pulse. The actual devices are Signetics 74121 monostable multivibrators with both positive and negative edge triggering inputs. Since the actual FM burst is 12-μs long instead of 10 μs, the additional 2-μs of time delay used to suppress Fresnel ripple must be removed from the signal. To do this, two monostables were cascaded. Looking at the figure, the initial video pulse simultaneously drives the FM expander and the first monostable. Referring to Fig. 16b, the distance between transducers creates a differential time delay, $t_{d_{fhigh}}$, between the monopulse trigger and actual expander output; this corresponds to a 2-μs delay. Operating in this mode, the far end of the FM burst would be gated while the close end would be unaffected, leaving undesirable time extention and frequency content. To overcome this, a second monopulse was placed in cascade to trigger off the negative-going edge of the first monopulse output pulse to effectively delay the gating pulse. Approximately 1 μs at each end of the burst is identically gated. This also eliminates any electromagnetic feedthrough due to packaging which may interfere with timing in following sections of the radar.

TABLE II - PULSE COMPRESSION SYSTEM OPERATING PARAMETERS

PARAMETER			
Power:	Dual supply:	-18V.	(White)
	Regulated	+12V.	(Red)
		Gnd	(Blk)
Transmitter:			
INPUT:	Video pulse		
	5 V, 8-15 ns, 70 KHz (variable)		
OUTPUT:	Rectangular		Hamming
Voltage (pp.)	100 mV		100 mv
Center freq.	60 MHz		60 MHz
Bandwidth	10 MHz		10 MHz
Amplitude flatness	±.75 dB		±.5 dB
Pulse length	10 μs		10 μs
Receiver:			
		FM Burst	
INPUT:	Rectangular		Hamming
Gain	+20 dB		+20 dB
Sidelobe level	-18 dB		-27 dB
Filtered	-20 dB		NA
Triple transit	-12.5 dB		NA
-4 dB Pulse width	205 ns		172 ns

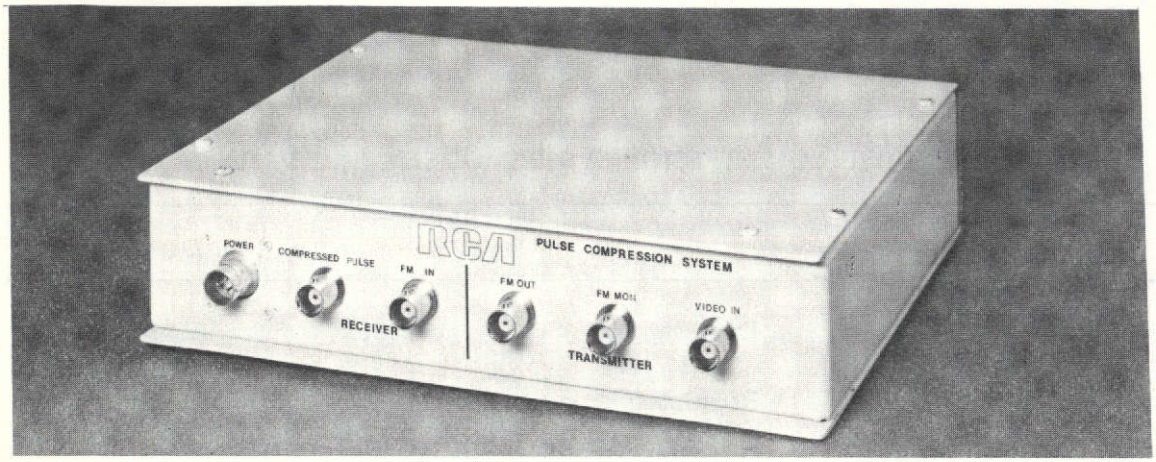

a) Complete package view.

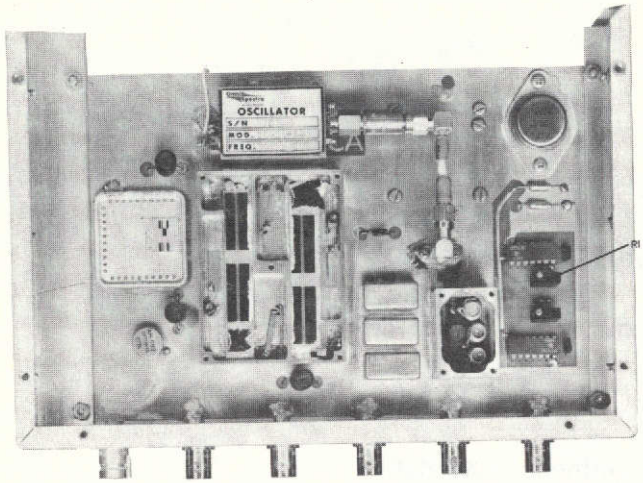

b) Top of circuit board.

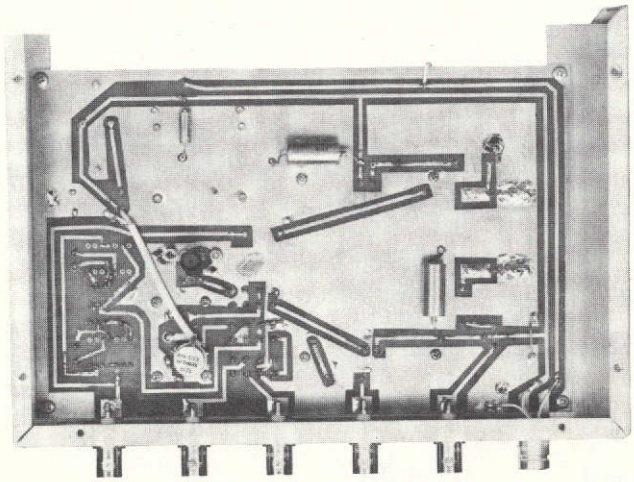

c) Bottom of circuit board.

Fig. 3. Pulse compression system.

An Omni-Spectra R8651-14 mechanically tuned oscillator provides a stable 120-MHz frequency source circuit. A complete parts list for the gate/limit circuitry is given in Table III along with the function of each part.

OPERATING INSTRUCTIONS FOR THE PULSE COMPRESSION SYSTEM

To operate the system, the following equipment is required:

HP 8008A Pulse Generator (or equivalent)
200-MHz Oscilloscope
HP 6205B Dual Power Supply

The operating procedure is outlined as follows:

1. Hook up the power supply to run in the + and - mode with a common ground. Set the positive supply to 10 V and the negative supply to 18 V. Connect the power to port labeled "Power" with the power cord provided (Red = +, Black = ground, White = -). See Fig. 3a for panel layout.

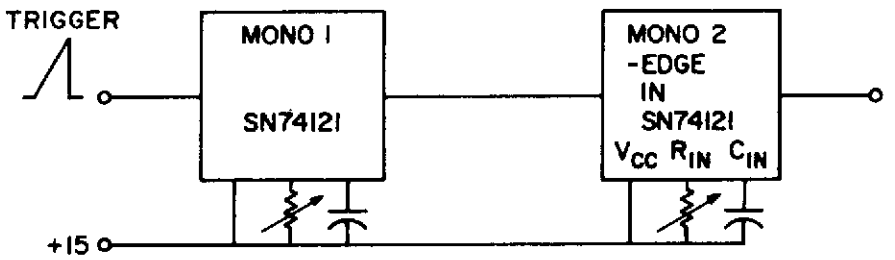

a) Monostable timing circuit.

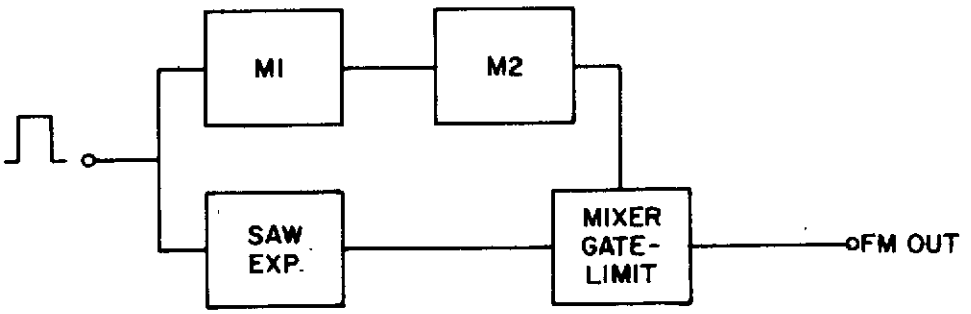

b) Block diagram of gate/limit operation.

Fig. 4. Gate/limit circuitry.

TABLE III - COMPLETE PARTS LIST FOR THE GATE/LIMIT CIRCUIT

Part Designation	Qty.	Part Description	Application
ET24P104	4	MEPCO/Electra 100 k Ω 3/8-in sq. trimpots	Timing resistors Limiting resistors Local Oscill. load
SN74121	2	Monostable Multivibrator 14-pin DIP	Gate/Limit pulse
AM-592	2	12-dB RF amplifier Optimax, Inc.	Amplification for weighting filter and mixing circuit
FMA70	2	Fairchild 50-90 MHz Amplifiers 47-dB gain	Amplification for SAW device
Johansen Air Gap 5202	3	Capacitors 0-10 pF	RF filter
SRA-1	2	RF mixers .5-500 MHz +7 dBm local (mini circuits)	Mixing gating/limiting
SRA-2	1	.1-400 MHz power splitter-combiner	Divides signal into monitor and transmit
LM309k	1	+5 V regulator Signetics	Power supply
132158 Coil	1	Inductor 6 1/2-turn #22 gauge	RF filter
CK05-8X-821K	2	Ceramic capacitors	Timing circuit

Note:

Extra capacitors for filtering purposes and inductors for matching the SAW lines to the RF amplifiers may be added where required.

2. Apply a 5-V p.p., 10-ns wide, 70-kHz repetition rate video pulse from the generator to the port labeled "Video In." Observe the output on 50-ohm scope at port labeled "FM MON." Adjust pulse width slightly until 10-μs pulse resembles Fig. 13a.

3. Connect the "FM Out" port to the "FM In" port with a short BNC cable. Observe output on scope at port labeled "Compressed Pulse." If sidelobes are not symmetrical or the pulse is distorted, adjust the local oscillator via the hole on the back panel.

4. To obtain a flat pulse, replace 1/8-W resistor (R1) indicated in Fig. 3b with one of the 50K trim pots taped to the rear panel, then adjust pot until the pulse shown in Fig. 2b is obtained.

5. To use the external filter, simply unsolder the 18-ohm resistor and coaxial cable.

MEASURED PERFORMANCE OF THE PULSE COMPRESSION SYSTEM

The measured frequency spectrum of the expanded pulse before gating and limiting shows the weighted response with a center frequency loss of 10 dB as shown in Fig. 5. This value is approximately 3-dB less than the predicted performance. A graphical representation in Fig. 6 compares the theoretical Hamming function to the normalized amplitude response. Figure 7 shows the triple transit pulse of the expansion line with a reference pulse 23 dB down from the peak. It can be seen in Fig. 8 that the amplitude ripple fills in after 6 μs when the triple transit pulse begins. Hard limiting the pulse removed the weighting and produced a square transmitting pulse in Fig. 9a with the frequency spectrum shown in Fig. 9b. Amplitude ripple was held to $\pm$.75 dB.

In the compression mode, velocity and phase errors are evident in the unsymmetrical sidelobe structure and nominal -18 dB suppression indicated in Fig. 10a. The null width obtained from Fig. 10b is 150 ns, 50-ns wider than the theoretical value for a 100:1 compression ratio. Further Hamming weighting imposed by an external filter in Figs. 11a and b produces an additional 2-dB sidelobe suppression, but also causes severe triple transit response at -12.5-dB below the peak.

Looking at the frequency spectrum of both the filter response in Fig. 12a and the compressed pulse spectrum in 12b indicates a center frequency shifted to 62.5 MHz. The ripple in the filter's passband indicates excess parasitic capacity in the packaging approach. The filtered pulse has a null width of 205 ns, slightly over the 200-ns specification.

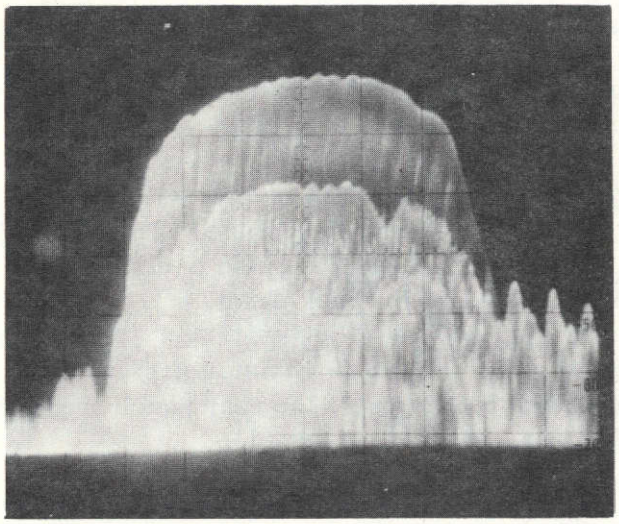

2 MHz/div
10 dB/div

Fig. 5. Frequency spectrum of pulsed delay line (f_c = 60.6 MHz).

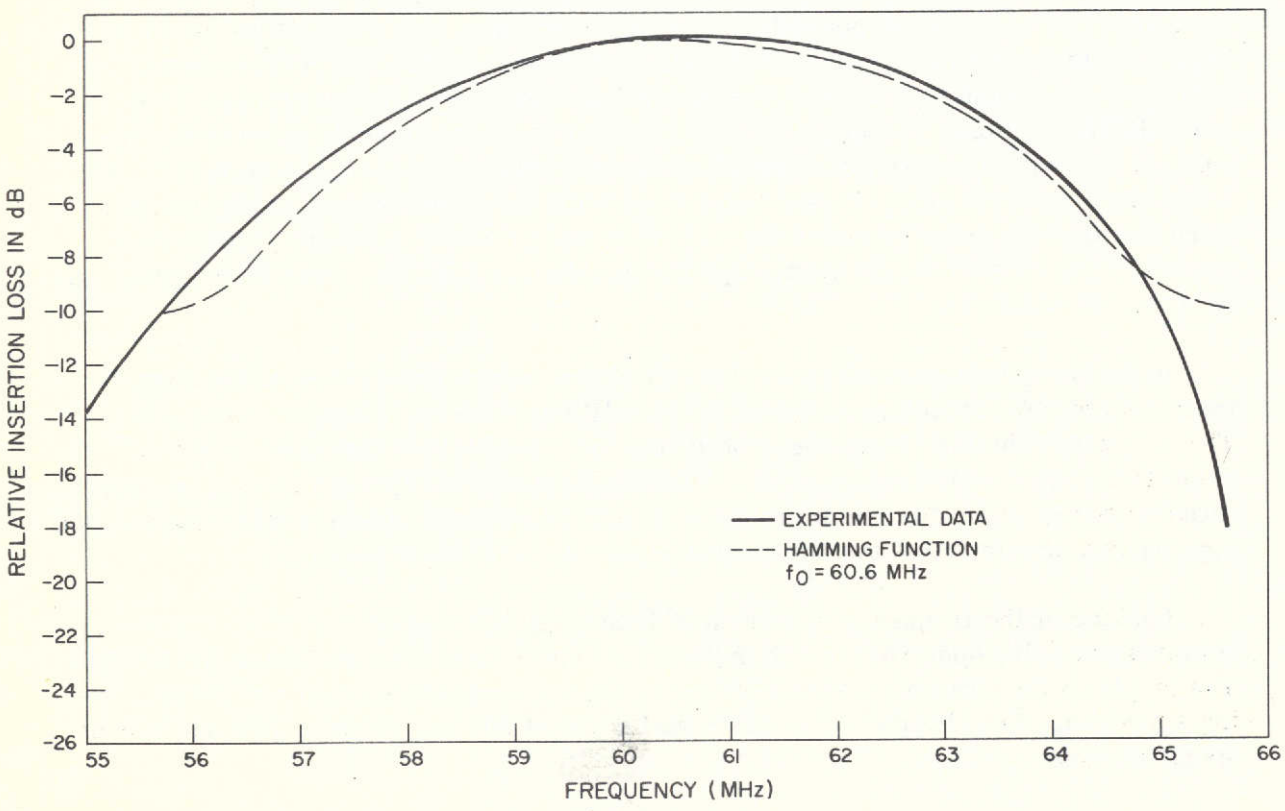

Fig. 6 Insertion loss characteristics of a Hamming weighted FM line.

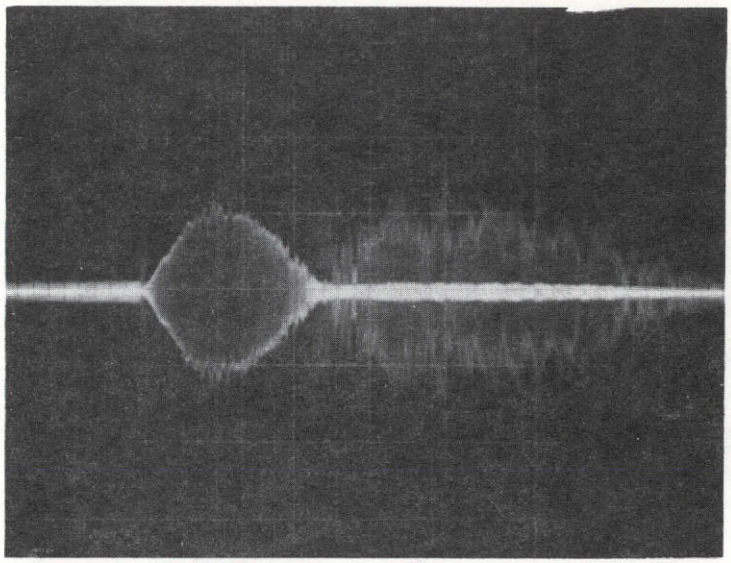

Fig. 7. Triple transit response with a -23-dB reference pulse.

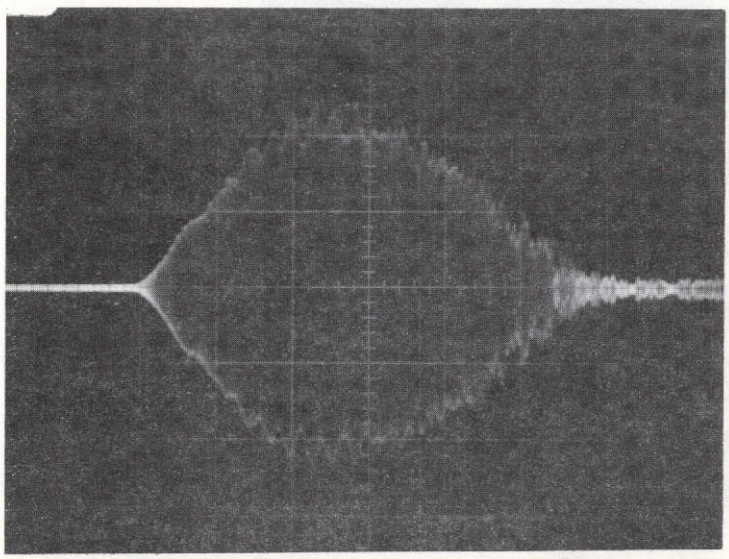

2 μs/div
.1 V/div

Fig. 8. Video pulse response of a delay line with Hamming weighting.

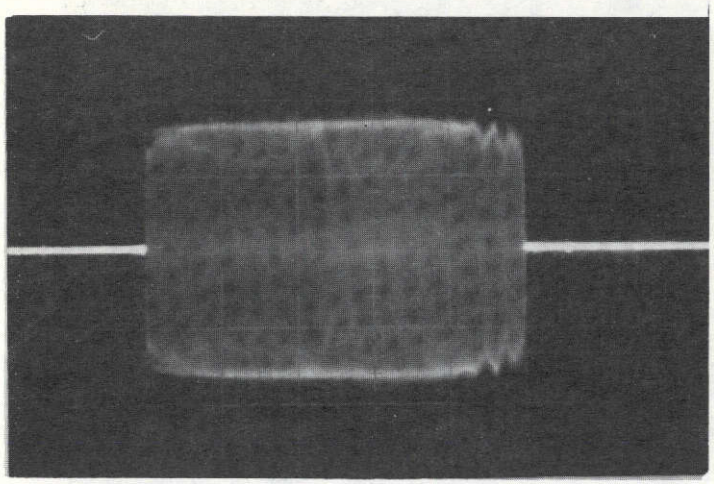

Fig. 9a. Gated and limited FM burst.

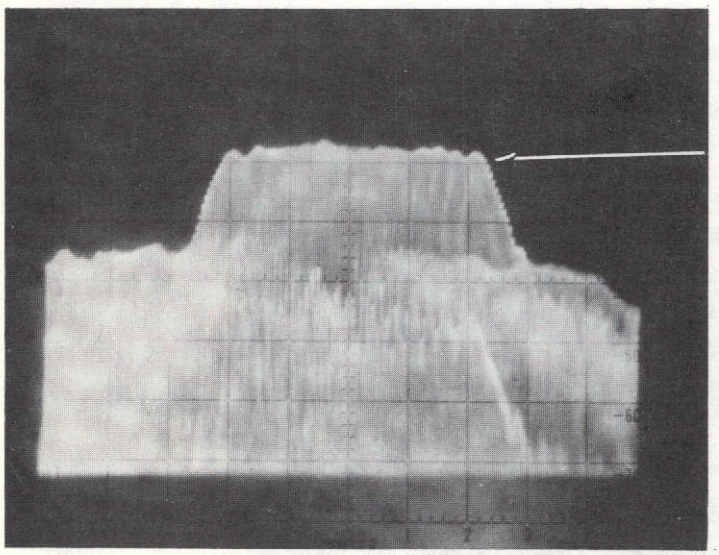

Fig. 9b. Frequency spectrum of limited pulse showing ±.75 dB ripple (f_c = 60.6 MHz).

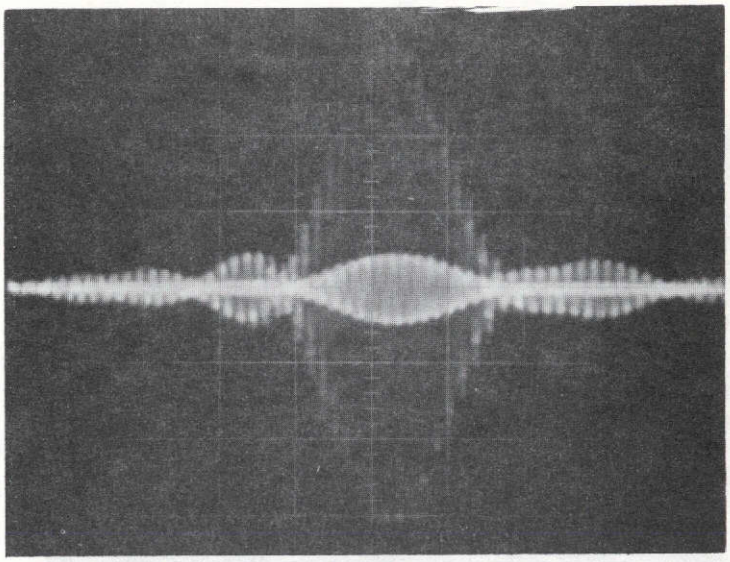

Fig. 10a. Compressed pulse with -18-dB reference pulse.

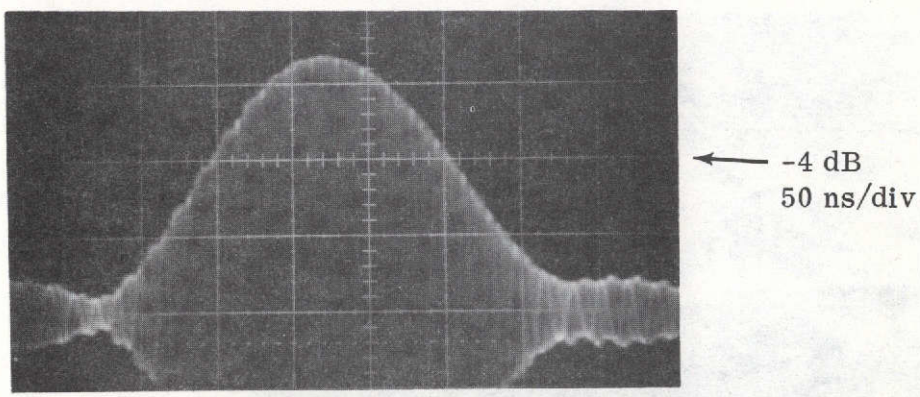

Fig. 10b. Expanded compressed pulse showing 150-ns, -4-dB pulse width.

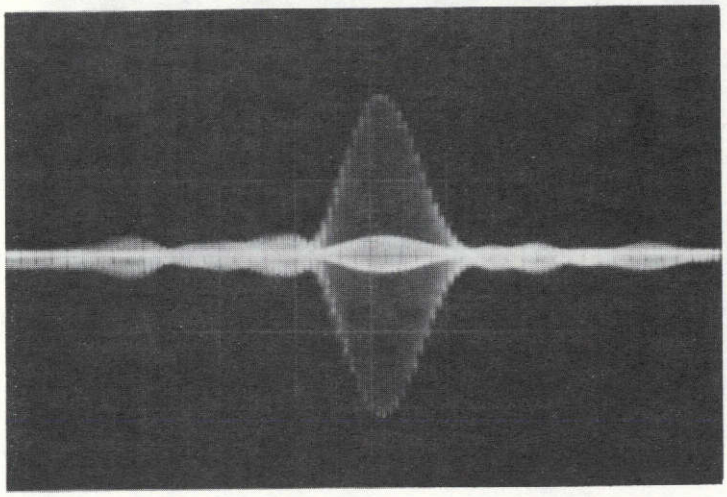

Fig. 11a. Filtered compressed pulse with -20-dB reference level.

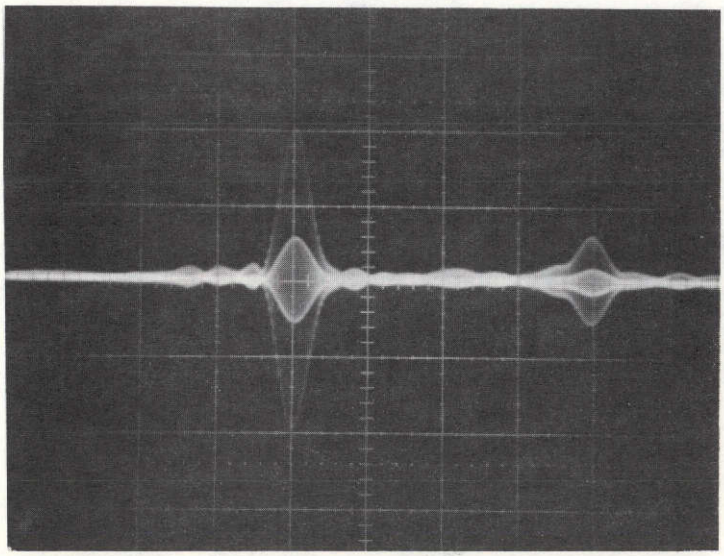

Fig. 11b. Triple transit response of weighting filter.

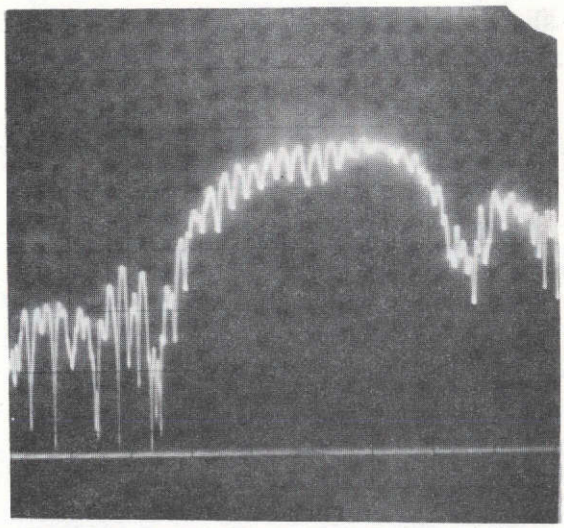

2 MHz/div
10 dB/div

Fig. 12a. Swept frequency response of Hamming weighted filter (f_c = 62.6 MHz).

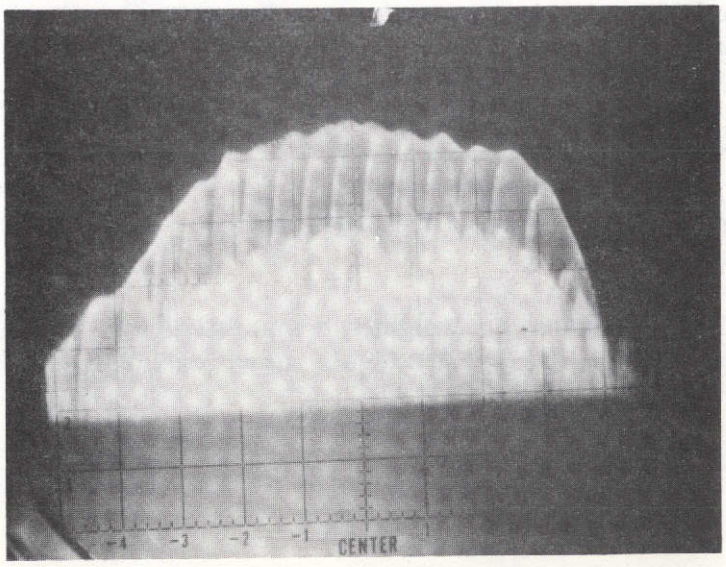

Fig. 12b. Filtered compressed pulse frequency spectrum (f_c = 62.5 MHz).

An alternative approach, however, uses a weighted transmitted pulse in a low power laboratory application. By unlimiting the expanded pulse, the original Hamming weighting help suppress the time sidelobes to -27 dB in the receiver with a pulse width of 172 ns. Figure 13a shows the transmitted pulse, while Fig. 13b compares the sidelobe level to a -27-dB reference pulse.

PERFORMANCE EVALUATION

The insertion loss of -10 dB midband closely matched the -12.6-dB theoretical value. The deviation occurs with the added response of the additional finger pairs at the same frequency, which is not accounted for in the computer analysis program. As previously noted, the amplitude closely follows the theoretical Hamming response within 1 dB until the band edges contribute diffraction losses and spurious bulk wave interference. The 10-MHz bandwidth would produce a 100-ns null width in the compressed pulse, but the Hamming function widens the pulse by a factor of 1.47. The measured 150-ns -4-dB null width corresponds to theory. The frequency/time decorrelation problem inhibited the Hamming function from producing the expected -30-dB sidelobes. Consequently, a square transmit pulse produced a -18 dB sidelobe level in the receiver. To determine the contribution of the stepwise linear approximation to the high time sidelobes would require extensive programming with Mason equivalent circuits. This technique was not available to aid the design.

The center frequency of the weighting filter turned out to be shifted 2-MHz higher than the center frequency of the expansion and compression lines; thus, the filter only suppresses the sidelobes an additional 2 dB and increases the -4-dB null width by 35 ns. As seen in Fig. 12b, the pulse frequency spectrum rolls off the lower frequencies beginning at 60 MHz. The swept frequency spectrum shows the same high sidelobes in the high frequency scale due to longitudinal bulk waves which the canceller does not affect. The filter insertion loss increased with feed-through and parasitic capacitance from a theoretical 15 dB, thereby decreasing the available sidelobe levels normally obtainable with a SAW filter. Figure 14 shows a conventional response with an earlier version of the weighting filter without bulk wave cancellation, but with excellent packaging.

The combined responses of a weighted transmitted pulse with a weighted transducer reduced the sidelobes to -27-dB levels but with a wider -4-dB null width of 172 ns.

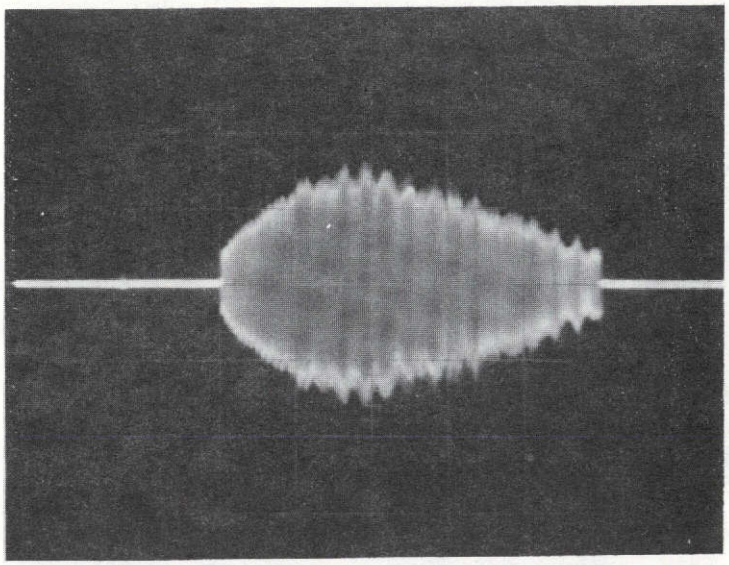

50 mV/div
2 μs/div

Fig. 13a. Hamming weighted transmitted pulse for low power application.

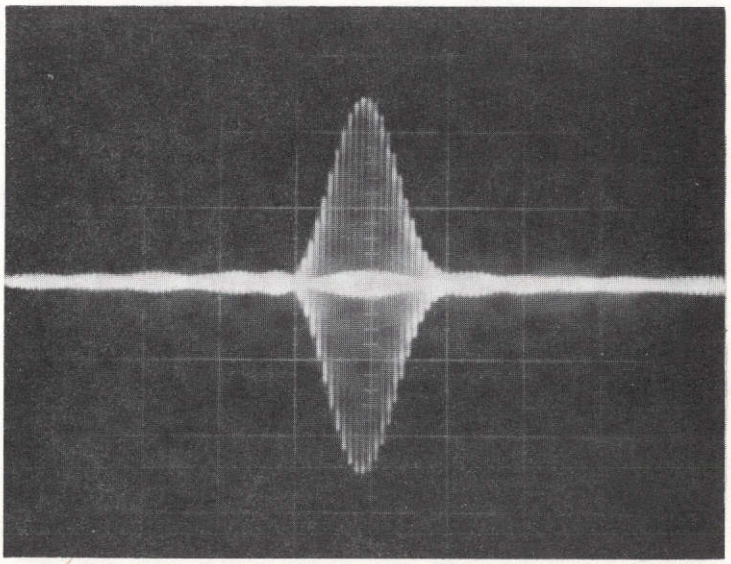

.2 μs/div
-27 dB ref pulse
.2 volt/div

Fig. 13b. Compressed pulse with -27-dB sidelobe rejection and no triple transit response.

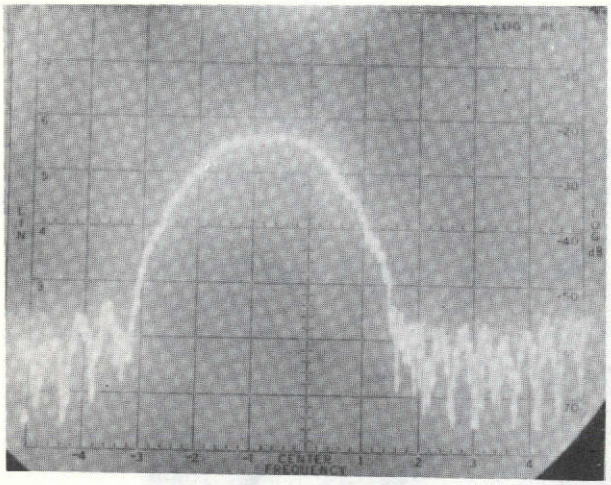

2 MHz/div
10 dB/div

Fig. 14. Swept response of an early version of the weighting filter.

THEORETICAL DESIGN OF DISPERSIVE FILTER

MATERIALS CONSIDERATIONS

Since the properties of the propagation media directly influence the design approach, the initial step is to select the substrate material. In brief, the four pertinent properties are propagation velocity, piezoelectric coupling coefficient, propagation loss, and temperature coefficient of time delay. More explicitly, the propagation velocity (V_o) determines the acoustic wavelength and transducer geometry, and thus bears directly upon fabrication limitations. The piezoelectric coupling coefficient affects the overall efficiency of the device in transferring energy from the surface to a metal electrode resting upon it and vice versa. More clearly, this factor indicates the ability of the transducers to convert electromagnetic signals into acoustic surface waves and then acoustic to electromagnetic waves at a later time, thus a determining factor in the overall insertion loss. The propagation loss factor indicates how much energy will be used to propagate a certain distance at a specified frequency. This affects the geometrical design of the transducer. Lastly, the temperature coefficient of time delay relates the stability of the time delay, frequency, and bandwidth of the device over a specified temperature range. Table IV summarizes the values of these properties for all the applicable substrate materials.

TABLE IV - PROPERTIES OF SOME SURFACE WAVE MATERIALS†

Material	Orientation	Velocity (cm/sec)	Coupling Coefficient (k^2)	Temp. Coefficient (α_T) (/°C)	Propagation Loss (100 MHz) (dB/μs)
AlN	C-axis	$6.1X10^5$	$\cong 0.5X10^{-2}$*	-	$\cong 0.15$
$LiNbO_3$	X-Z	$3.8X10^5$	$0.24X10^{-2}$	$93X10^{-6}$	0.01
$LiNbO_3$	Y-Z	$3.48X10^5$	$4.4X10^{-2}$	$94X10^{-6}$	0.01
Quartz	ST-X	$3.16X10^5$	$0.11X10^{-2}$	0	0.03
ZnO	C-axis plate	$2.7X10^5$	$\approx 0.7X10^{-2}$*	-	$\cong 0.1$
$Bi_{12}GeO_{20}$	Z cut	$1.62X10^5$	$0.74X10^{-2}$	-	0.05

*For a thickness-to-wavelength ratio of 0.045.
†Values provided by T.A. Szabo and A.J. Slobonik [1].

Since the pulse compression system will be primarily used in a laboratory environment with a relatively constant temperature and with a low insertion loss figure, $LiBNO_3$ was selected as the substrate material to take advantage of its low propagation loss, high coupling coefficient, and high velocity to meet insertion loss and fabrication requirements. If a large operating temperature range were required, ST-cut quartz would have been selected.

INTERDIGITAL TRANSDUCERS (IDT)

Once the material is selected, a transducer geometry is chosen to exploit the unique ability of the surface wave to localize energy on a free surface, thus allowing different sensors to simultaneously sample the signal. In other words (referring to Fig. 15), since the signal remains on the surface for the complete delay time, differently located sensors along the delay path can sample the waveform at the same time. As shown in Fig. 15, a pair of interdigital fingers form the basic sensor. From the illustration, each finger is located at π-radian intervals corresponding to positive and negative voltage peaks. In this way, the finger pair extracts energy from the wave traveling under it, but is sensitive only to signals with acoustic wavelengths twice the spacing between finger centers. So by simply altering the spacing between adjacent interdigital pairs, a transducer will be sensitive to different frequencies at different points along the delay path. Clearly then, by varying the spacing according to a linear FM equation the transducer will effectively sample and produce an FM signal. The standard FM equation used to position the electrodes is as follows [2]:

$$X_n = V_R \left[\frac{\Delta F \cdot F_o}{\Delta T} \left(1 - \sqrt{1 - \frac{n \Delta F}{F_o^2 \cdot \Delta T}} \right) \right] \qquad (1)$$

from $M \leq n \leq N$,

where:

V_R = free surface velocity

ΔT = pulse length (delay time) μs

Δf = bandwidth (MHz)

F_o = center frequency (MHz)

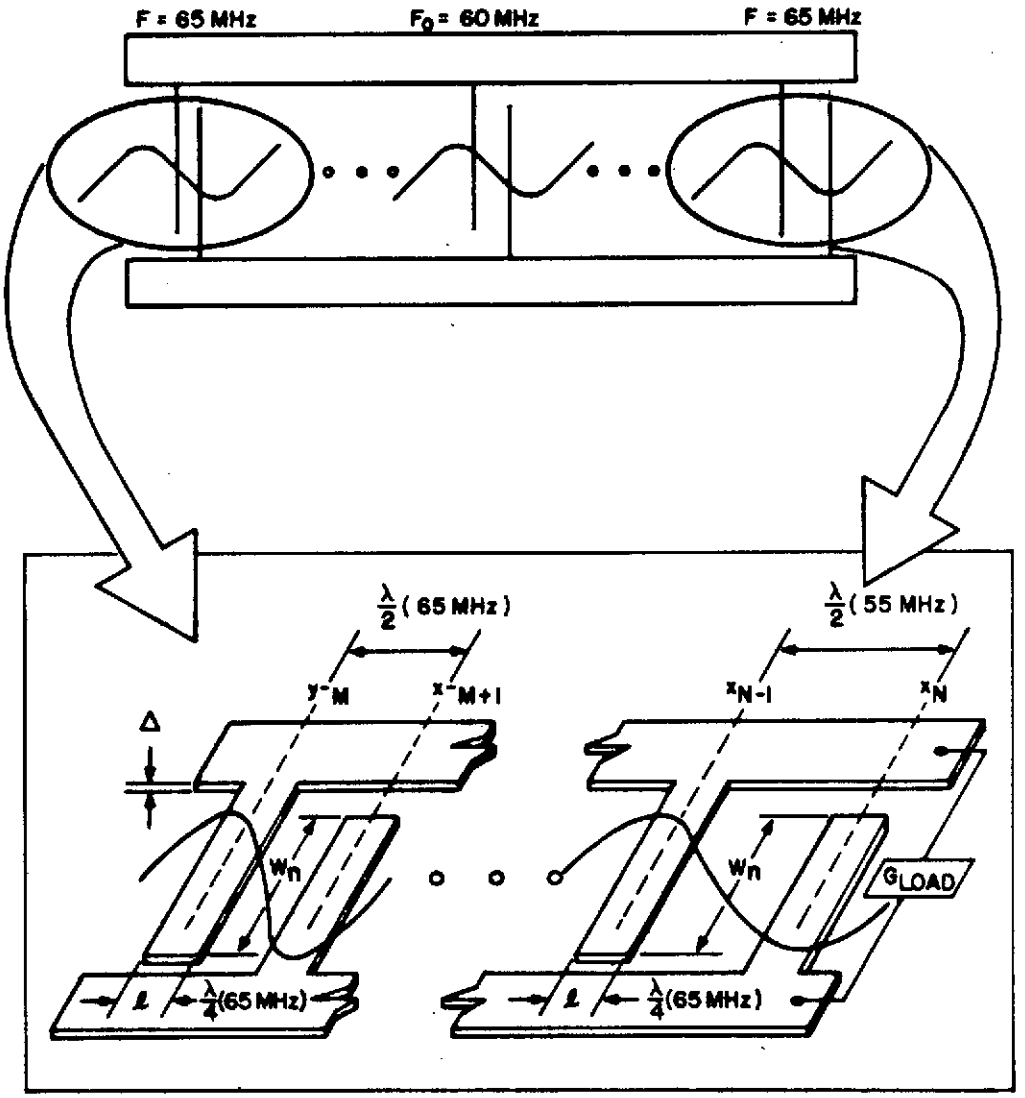

Fig. 15. Electrode position in the dispersive transducer.

$$M = F_o \cdot \Delta T + \frac{\Delta F \cdot \Delta T}{4}$$

$$N = F_o \cdot \Delta T - \frac{\Delta F \cdot \Delta T}{4}$$

n = finger number

ACOUSTIC REFLECTIONS

Care must be taken in what sequence the frequency is varying, due to physical interaction between the wave and the fingers. More specifically, a finger pair represents an impedance discontinuity to a wave traveling in a high coupling material such as $LiBNO_3$. In a transducer whose geometry varies with frequency (Fig. 16a), the reflections will increasingly suppress the coupling of any surface wave energy traveling toward the lower frequency electrodes. In other words, a surface wave generated by electrodes spaced by a distance d will be increasingly reflected as it travels under fingers spaced greater than d apart. The reason for this is the coherent conversion of a portion of the wave energy to a sheer wave traveling away from the surface as viewed in Fig. 17. Furthermore, the proper condition for back-scattered waves excited by a surface wave may be given by [3]:

$$\theta = \cos^{-1}\left(\frac{V_S}{d \cdot f} + \frac{V_S}{V_R}\right). \tag{2}$$

Consequently, to produce the best possible linear FM waveform, the line was designed with the finger spacing increasing with time delay or in a "down-chirped" mode.

TRANSDUCER GEOMETRY

The "down-chirp" mode, however, can be generated by two different transducer geometries designated as single dispersive and double dispersive [4] as shown in Fig. 16a and 16b, respectively. The single dispersive line uses a small launching transducer with equally spaced finger pairs with adequate frequency response to deliver relatively equal power over the dispersive bandwidth.

The bandwidth at the launch transducer is determined by equation (3) below [5].

$$BW\ (-3\ dB) = \frac{f_o}{N} \tag{3}$$

f_o = center frequency

N = number of finger pairs

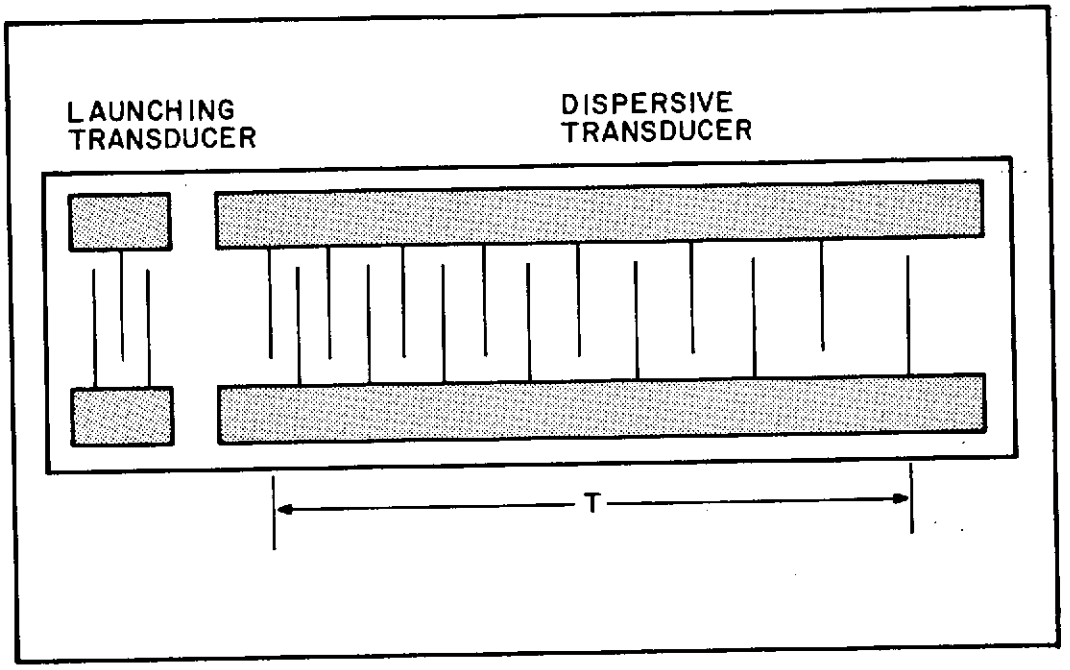

a) Linear FM single dispersive transducer.

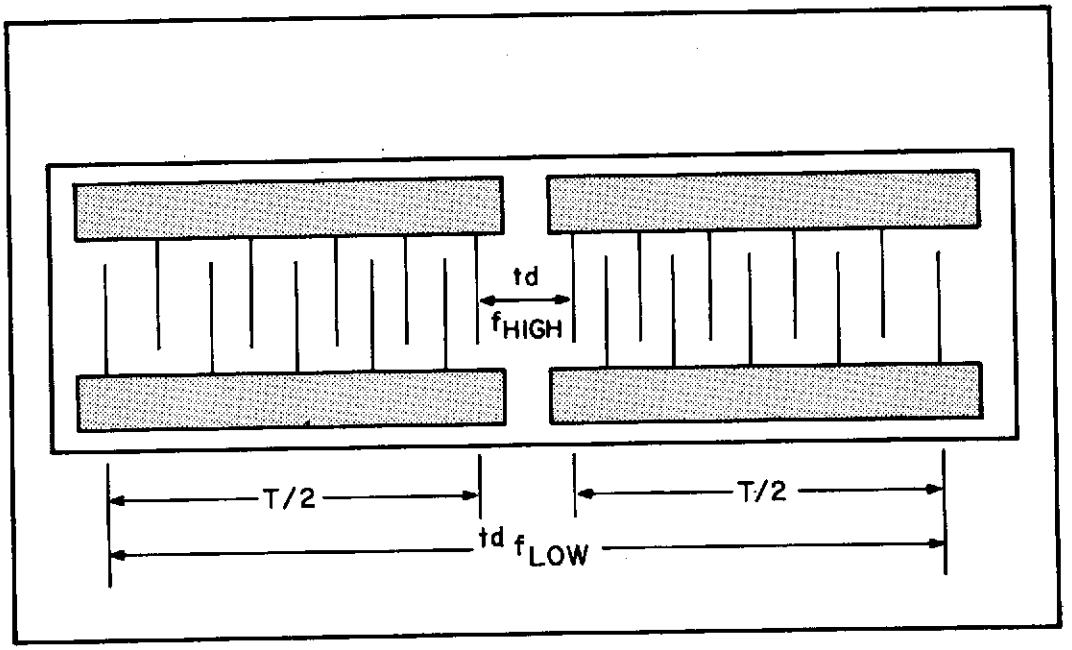

b) Linear FM double dispersive transducer.

Fig. 16. Transducer geometries.

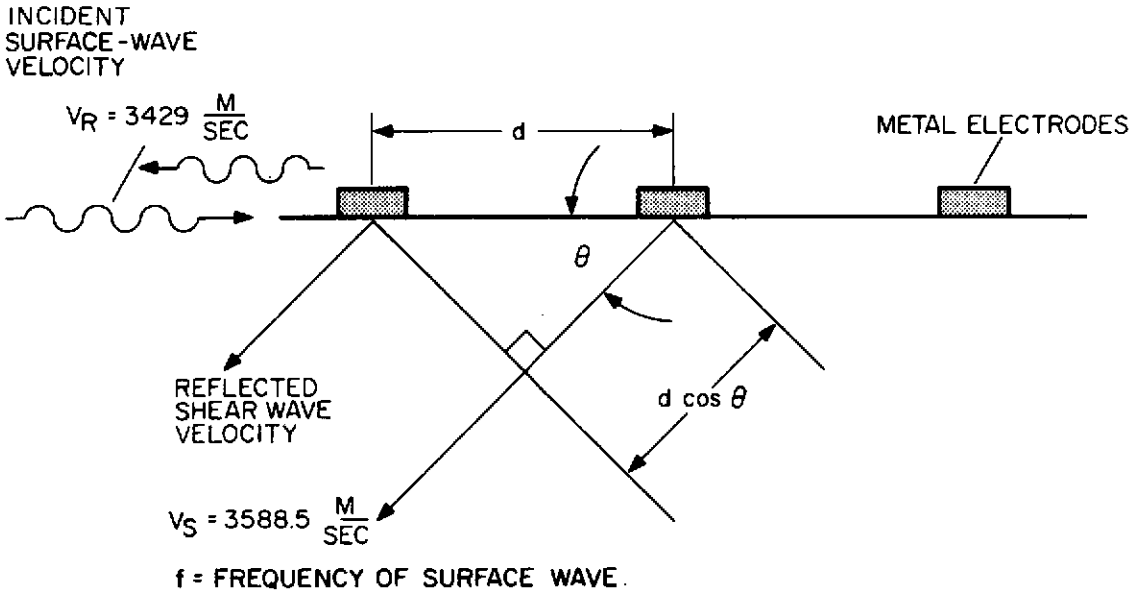

Fig. 17. Coherent mode conversion of surface-waves to shear waves.

A surface wave is launched by impulsing the nondispersive line with a video pulse, then by taking the signal out of the dispersive transducer a linear FM burst is obtained.

In the double dispersive line, Fig. 16b, two transducers with half the delay time but full bandwidth add delay time to generate the full FM burst. One transducer is impulsed, launching specific frequencies from the respective finger positions along the input transducer, while an inverted identical transducer extracts the high frequencies first and delays the lower frequencies. This technique creates an expanded pulse of twice the single dispersive transducer delay time. But since the launching finger number and aperture are appreciably smaller than the single dispersive launcher, the line suffers increased insertion loss. The initial approach utilized the single dispersive transducer line with excellent results. However, the double dispersive geometry was employed when fabrication problems imposed design limitations. This will be discussed in more detail in the section on artwork generation.

STRONG COUPLING MATERIAL DESIGN

Although the strong coupling capability of $LiBNO_3$ reduces insertion loss, the effect of placing metal electrodes upon the surface produces undesirable variations in the surface wave velocity. Strong coupling means that an intense electric field travels along the surface with the wave, not only inducing current within the metal fingers as the wave passes, but interacting with nearby undisturbed surface. Also, this interaction produces an apparent "stiffening" of the surface, thus increasing the velocity of the surface wave[6]. Moreover, when the wave travels under a finger, the metal effectively shorts out the accompanying electric field, thereby reducing the surface tension and slowing the velocity. Once out from under the finger, however, the wave speeds up again with the aid of the field. This process occurs with each metal electrode and could be treated easily if the electrode widths and spacings were equal. Present fabrication processes, however, require the finger width to be held constant, while in a dispersive array the spacing is varying according to the FM equation. Clearly, as the spacing varies for each finger, the "effective" velocity will be slightly different, thereby producing erroneous electrode placement. To adjust for this phenomenon an equation developed by Sittig [3] provides a correction factor to each electrode position. Equation (4) actually represents the simultaneous solution of three contributing equations [7]:

$$X_n = \left\{ X^2 + (m-1) \cdot Y \right\}^{1/2} + (m-1) \left\{ 1 - \frac{V_o}{V_m} \right\} \ell \qquad (4)$$

$$n = 1, 2, 3, \ldots N$$

where:

$$X = \frac{V_o}{2} \left(F_{Min} \cdot \frac{\Delta T}{\Delta f} - \frac{1}{2 F_{Min}} \right)$$

$$Y = \frac{V_o^2}{2} \frac{\Delta T}{\Delta f}$$

V_o = free surface velocity

ΔT = time delay

Δf = bandwidth

ℓ = finger width

One of the contributing equations relates the frequency to its overall group delay time. The second contributing equation simply defines the frequency of the nth electrode, and the third calculates the time delay to the centroid of the nth electrode as a function of the "effective" velocity of the first n electrodes. This correction factor turns out to be approximately 1% across the band.

The second consideration is the wave dispersion occurring under the electrodes because of their finite thickness [3] which relates directly to the calculation of V_m in equation (4). The relationship defined below is an empirical determination of the actual velocity:

$$V_m \text{ (metallized velocity)} = V_o - \lambda h f \tag{5}$$

where:

f = frequency

λ = 0.28 (Al on $LiBNO_3$)

h = 1500 Å (electrode thickness)

This velocity is expressed as a linear dependence on frequency. Moreover, the very presence of a mass of metal on the surface of the material shorts the electric field and effectively lowers the overall surface velocity. Extensive investigation of this effect made by Williamson [8] found that an interdigital array on $LiBNO_3$ would reduce the free velocity about 1.6% or approximately 56 m/sec. This fact was verified with the first experimental line produced for this contract. The actual center frequency and bandwidth obtained corresponds to a velocity reduction of approximately 1.5% indicating an incorrect design velocity.

APODIZATION

Another feature of the interdigital array involves altering the amount of overlap between fingers to compensate for various degrading effects or to produce desired amplitude responses. One such effect is the non-uniform extraction of energy resulting in a tapered frequency spectrum. The reason for such tapering is that the number of active fingers decreases with frequency, thereby extracting less energy at lower frequencies. Figure 18 illustrates the necessity of electrode overlap compensation.

The frequency dependence is shown in equation (6) below[7]:

$$na(f) = 2\left(\frac{f}{\Delta f}\right) \sqrt{\Delta T \cdot \Delta f} \tag{6}$$

To compensate for this effect, equation (7) adjusts the finger overlap to level the amplitude response of the device:

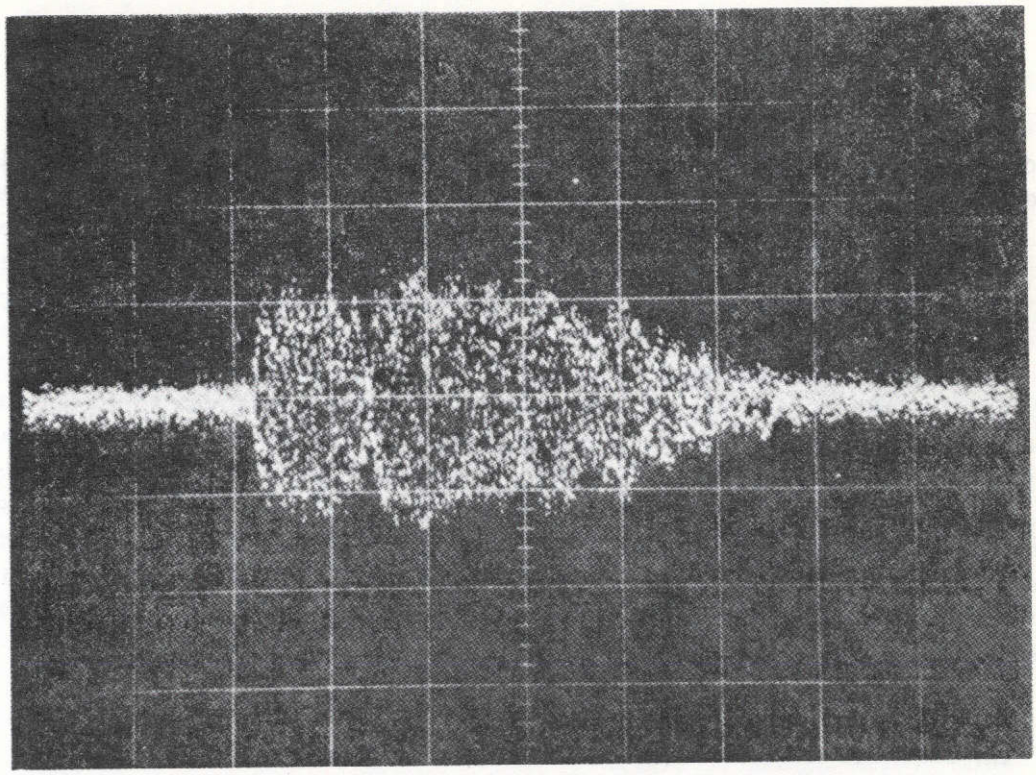

Fig. 18. Amplitude taper of an unapodized linear FM transducer.

$$W_n = \frac{W_o}{2} \left[\frac{\left(1 + \left(\frac{f_n}{f_o}\right)^2\right)}{\left(\frac{f_n}{f_o}\right)^3} \right] \cdot e(\tau) \qquad (7)$$

W_n = aperture in wavelengths @ f_n

f_n = frequency at nth finger position

f_o = center frequency

W_o = aperture in wavelength @ f_o

$e(\tau)$ = envelope shape factor

$n = 1, 2, 3 \ldots .$

W_o corresponds to the midband aperture whose value depends upon the external load (50 ohms) and diffraction characteristics of the transducer geometry. The value of $e(\tau)$ determines the shape of the FM burst which when set to unity defines a rectangular envelope. However, this factor changes to a cosine function in the matched filter section. The numerical calculations and graphs will be illustrated in the design section.

Recall that there are repetitive velocity variations of a surface wave as it passes under the metal electrodes due to the electric field being shorted. Consequently, if the aperture varies by a significant amount, portions of the wave will lag the surface wavefront where no electrode exists. The ultimate effect, as illustrated in Fig. 19a, will be to distort the wavefront and induce undesirable phase errors which cause high sidelobes in the compressed pulse. Figure 19b, however, shows that by inserting "dummy" electrodes into the areas where the fingers are shortened, the velocity will be equalized across the aperture, thus maintaining a relatively flat wavefront and phase response[9].

TRIPLE TRANSIT ECHOES

This section describes the phenomenon of coherent reflection (echo) and the design tradeoffs between insertion loss and the triple transit signals. As previously noted, wave detection occurs at each half wavelength of a wave at the proper frequency, but simultaneously part of the wave reflects down and backward (Fig. 17). So at each electrode, a backward-going wave forms in phase with the previous reflection, these waves then travel back to the original launching electrodes and reflect again. At any given frequency, the insertion loss for a single dispersive transducer is found from:

$$I_L = \frac{2Q_L Q_r}{(Q_L + Q_r)^2 + Q_L^2 Q_r^2}$$

where:

$$Q_r = \frac{\pi}{4K^2}\left(\frac{\Delta f}{f_o}\right); \quad Q_L = \frac{2\pi f_o C_T}{G_L}$$

and G_L is the load conductance. Also, the acoustic reflection coefficient,

$$\rho(W) = \frac{Q_L^2}{(Q_L + Q_r)^2 + Q_L^2 Q_r^2},$$

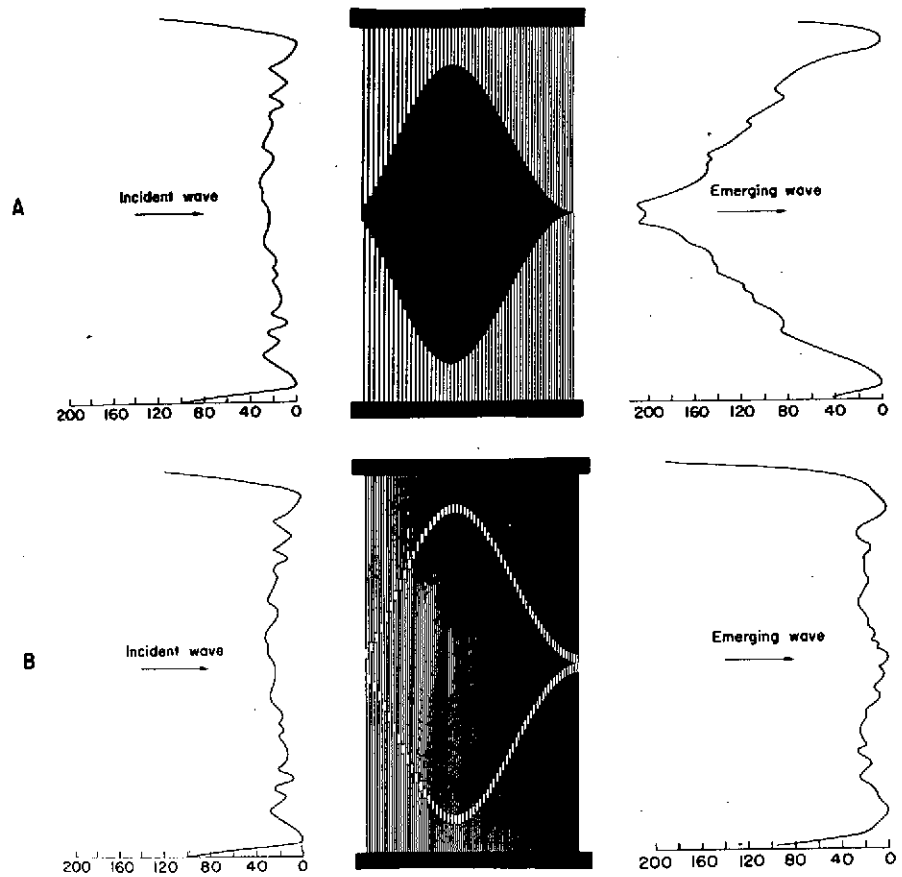

Fig. 19. Wavefront distortion as an acoustic wave incident from the left passes under: a) highly apodized IDT, b) highly apodized IDT with inserted "dummy electrodes" [9].

must be small ($<< 1$) to keep triple transit signal low. If $\rho(W)$ remains constant with frequency change, a third trip echo with a response similar to Fig. 20 is expected. Furthermore, since the point of reflection changes with frequency in a dispersive line, the triple transit echo stretches to three times the length of the original signal with an amplitude response simulating the apodization pattern. The echo signal, however, retains the same bandwidths; therefore, its chirp rate is one-third that of the original signal and will not efficiently compress in the matched filter. The net result is that the echo suffers loss due to reflection plus the "decorrelation" loss. For example, a decorrelation loss of 18 dB with a minimum triple transit isolation of 12 dB will provide a third time echo that is at least 30 dB down from the main signal.

In conclusion, the values of both insertion loss and reflection suppression depend on the coupling between the acoustic surface waves and the external load G_L. In order to drive the dispersive array most efficiently without restricting the bandwidth, $Q_L = 1$ is assumed, which for this design corresponds to a device impedance of 4 ohms. Therefore, a matching network is utilized to match to a 50-ohm generator source from the SAW device.

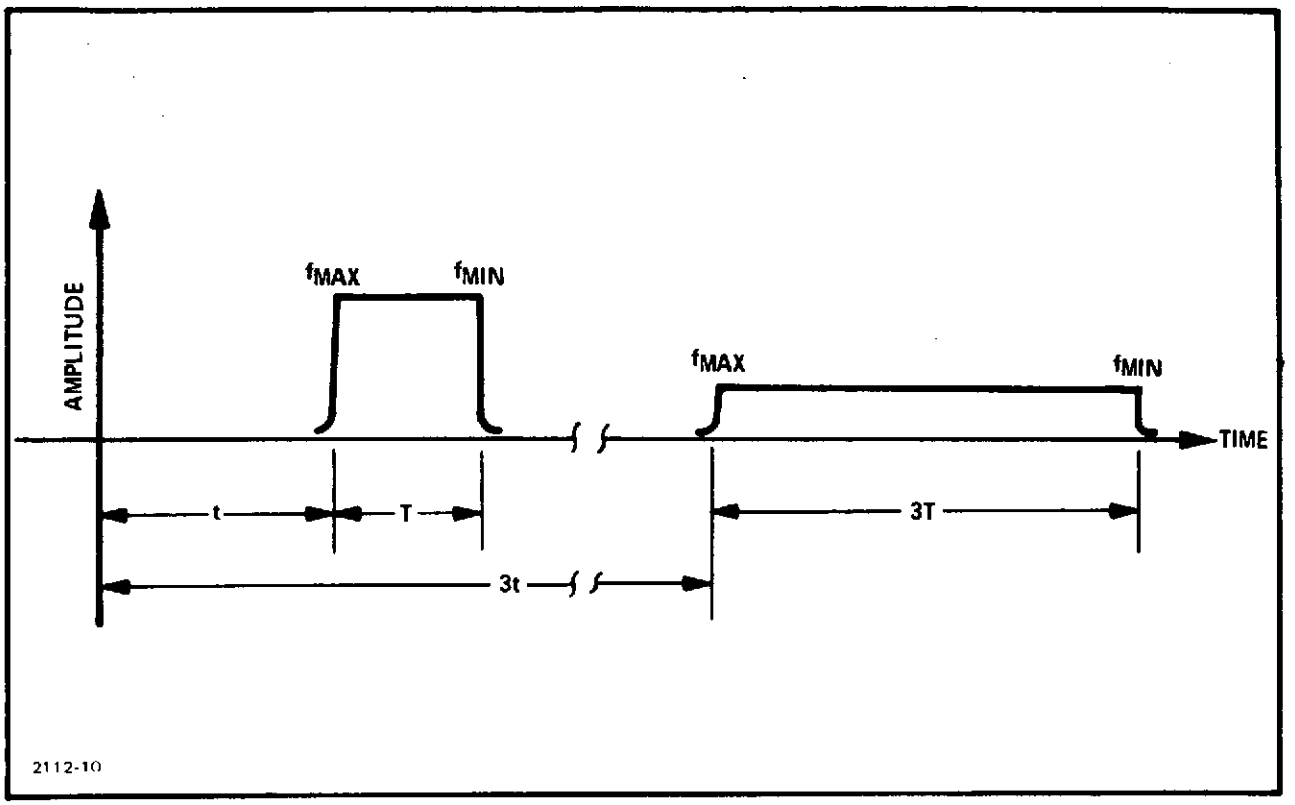

Fig. 20. Time domain response of the desired signal and its triple transit echo.

DIFFRACTION CONSIDERATIONS

Another contributing factor in amplitude response of the array is the loss caused by "beam spreading" of the wavefront. Diffraction of a surface wave affects the power delivered by increasingly widening the beamwidth with distance. The diffraction of the wave is determined by the equation below:

$$\theta \text{ (Beamwidth)} = W_s \lambda_o + \frac{2D}{W_s} \tag{8}$$

$$\text{D.E. (Diffraction Efficiency)} = \frac{W_R \cdot \lambda_o}{\theta} \tag{9}$$

where

W_s = sending electrodes finger overlap

W_R = receiving electrodes finger overlap

λ_o = synchronous wavelength (inches)

D = traveling distance of wave (inches)

Since in the double dispersive transducers one pattern is the mirror image of the other, the sending and receiving electrode overlaps are the same. Figure 21 illustrates the effect of "beam spreading" upon the power delivered to the receiving electrodes. Table V shows the values for aperture in wavelengths to obtain an equivalent diffraction efficiency across the band. The adjusted aperture equations to compensate for diffraction are listed below:

Frequency Range = 54 to 60 MHz:

$$W_n = \frac{W\left[1.32 + \left(.52 + .48\,\frac{f_R}{f_o}\right)^2\right] \cdot \left[2 - \frac{f_R}{f_o}\right]}{2\left(\frac{f_n}{f_o}\right)^3} \tag{10}$$

Frequency Range = 60-66 MHz:

$$W_n = \frac{W\left[1.32 + \left(.52 + .48\,\frac{f_n}{f_o}\right)^2\right] \cdot \left[1\text{-}2.5\left(1 - \frac{f_n}{f_o}\right)\right]}{2\left(\frac{f_n}{f_o}\right)^3} \tag{11}$$

In addition to the beam spreading, other effects such as acoustic wave guiding by the sum bars and fabrication limitations are not reflected in the adjusted equation.

FRESNEL RIPPLE

In addition to wavefront phase error, the phenomena of Fresnel ripple produces both amplitude and phase ripple whenever an abrupt frequency truncation in the Fourier transform occurs. This corresponds to abruptly ending a transducer which theoretically should have an infinite frequency response. Basically, the problem arises whenever residue quadratic phase terms in the Fourier transform are not cancelled by matched filtering. Table VI shows the effect of phase error upon the theoretical peak-to-sidelobe ratios [9].

Although no mathematical solution exists that provides a way to eliminate the residue phase terms, by adding a taper to the ends of the transducer (Fig. 22) to at least 15% of the total aperture width, the spectrum ripples are essentially eliminated [4]. This technique was implemented using the equation:

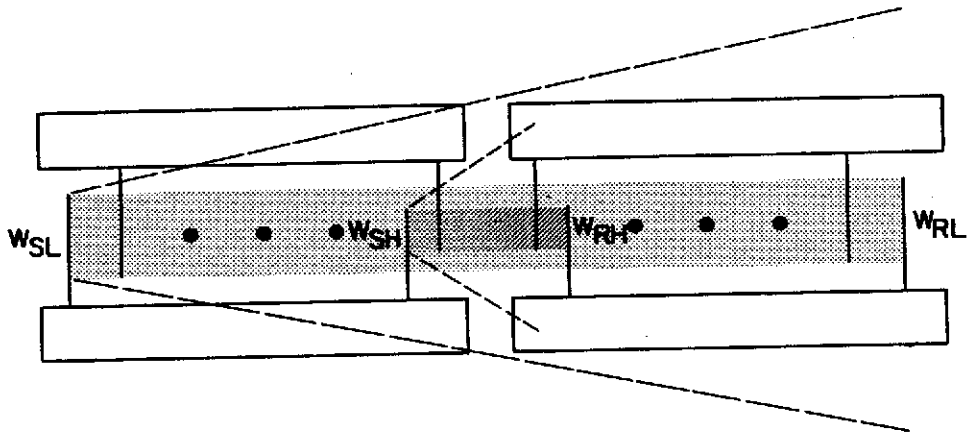

Fig. 21. Beam spreading effect at the extreme edges of the IDT.

TABLE V - DIFFRACTION EFFICIENCY

Freq (MHz)	Distance Traveled (in)	Diffraction Efficiency (%)	Aperture $W_n(\lambda)$
55	0.4	20.9	20.4
60	1.07	19.5	15.0
65	1.75	20.0	9.6

TABLE VI - SIDELOBE DEPENDENCE ON PHASE ERROR

Sidelobe Level (dB)	Fourier Phase Coefficient
20	±11.5°
25	±6.35°
30	±3.6°
35	±2.05°
40	±1.15°

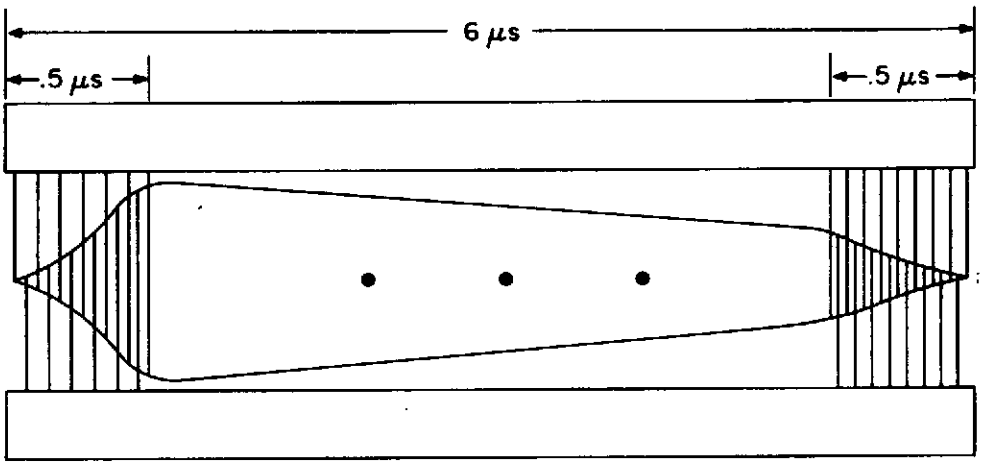

Fig. 22. Fresnel compensated transducer with 0.5-μs cosine squared taper on ends.

$$T(f) = \cos^2 \left\{ \frac{\pi (f - f_{min})}{2(f_{min} - f_d)^2} \right\} \tag{12}$$

f = frequency (MHz)

f_{min} = low cutoff

f_d = end frequency

f_h = high cutoff.

For the high frequency cutoff, simply substitute f_h for f_{min} in equation (12).

ELECTRICAL CHARACTERIZATION

Another useful design consideration involves modeling the interdigital structure by an equivalent electrical circuit. At present, the two theories for metal electrodes consider either normal (cross-field) or parallel (in-line) electric field configurations. Figure 23 illustrates the basic ideas involved. Since $LiBNO_3$ is the propagation medium, the high coupling factor (K^2) is best simulated using the cross-field model [10]. From this basic model, Mason [11] derived an electrical equivalent circuit for the acoustical response of an IDT pair. Figure 23 shows the circuit as a three part network for a single section, — a single electrical port with two acoustical ports to account for bi-directionality. The transit angle θ simulates the time delay through the section

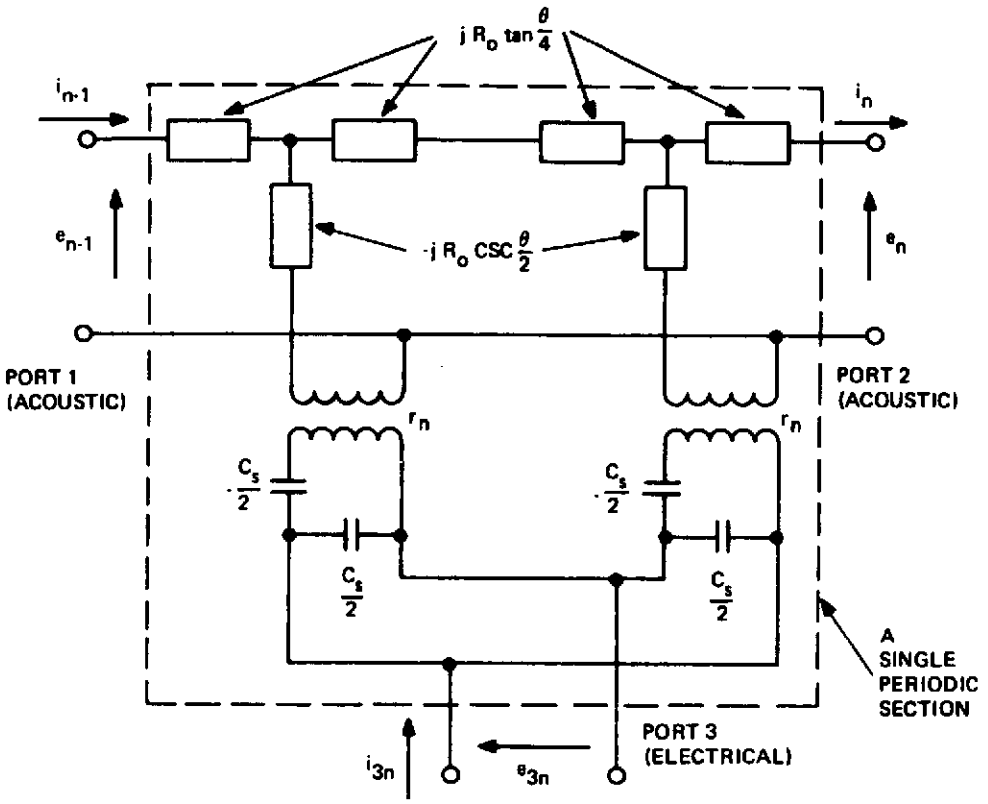

L = PERIODIC LENGTH

v = SURFACE WAVE VELOCITY

h = PIEZOELECTRIC CONSTANT

$f_o = \frac{v}{L}$ = SYNCHRONOUS FREQUENCY

$\theta = 2\pi \frac{\omega}{\omega_o}$ = PERIODIC SECTION TRANSIT ANGLE

C_s = ELECTRODE CAPACITANCE PER SECTION

k^2 = ELECTROMECHANICAL COUPLING CONSTANT

r_n = TRANSFORMER TURN RATIO

Fig. 23. Mason equivalent circuit for a single periodic section ("cross-field" model).

while the transformer coupling accounts for the electro-acoustic interaction, with r_n dependent upon the transducer geometry and material parameters. Hence, by cascading the model as indicated in Fig. 24, the entire array can be modeled and analyzed by a computer to provide phase-amplitude response data.

These calculations are complex and time consuming but provide useful data when novel schemes of transducer geometry, electrode placement, and weighting are involved. The approaches considered in this contract were formatted along previous successful attempts, with variations to handle the particular delay line parameters and characteristics.

One benefit derived from the electrical equivalent model is the simulation of the total array as a series of parallel networks to evaluate radiation immittance and capacitance. Figure 25 shows the two equivalent circuits. The shunt circuit proves to be the most convenient approach, since parallel electrodes form the basic IDT structure. The necessary design equations were developed by Smith et al [10] and are utilized in a dispersive radiation analysis program (DRAP) to calculate and sum individual finger pair conductance, susceptance, and capacitance across the array. The program output for this delay line appears in Fig. 26. The equations used for calculating the conductance Ga(w), and susceptance, Ba(w), are listed below:

$$Ga(w) = 2\, G_o\, (\tan\, \theta/4\, \sin\, N\, \theta/2)^2 \tag{13}$$

$$Ba(w) = G_o\, \tan\, \theta/4\, (4N + \tan\, \theta/4\, \sin\, N\theta) \tag{14}$$

where

$G_o = \frac{4}{\pi}\,(K^2 W_o C_s N^2)$

$\theta = 2\pi\, W_n/W_o$

W_o = radian center frequency

W_n = radian frequency of the nth electrode

The various constants are: $K^2 = 0.0482$, $C_S = 0.4$ pF, and $N = 600$, so G_o would equal 3 mhos. Also, the total capacitance of the array is the sum of the individual capacitances, $C_T = N\, \hat{C}_S = 107$ pF where $\hat{C}_S$ is determined in the program. For the Hamming weighted transducer, the total capacitance is approximately 60 pF. Ga(w) and Ba(w) are plotted in Fig. 27. These plots show that the radiation immittance varies slightly across the band and slopes on the ends. The sloping occurs as the number of active fingers decreases near the end of the transducer having fewer responding neighbors than the middle section of the transducer. This is illustrated in Fig. 28 with both the number of active fingers and conductance plotted as a function of frequency.

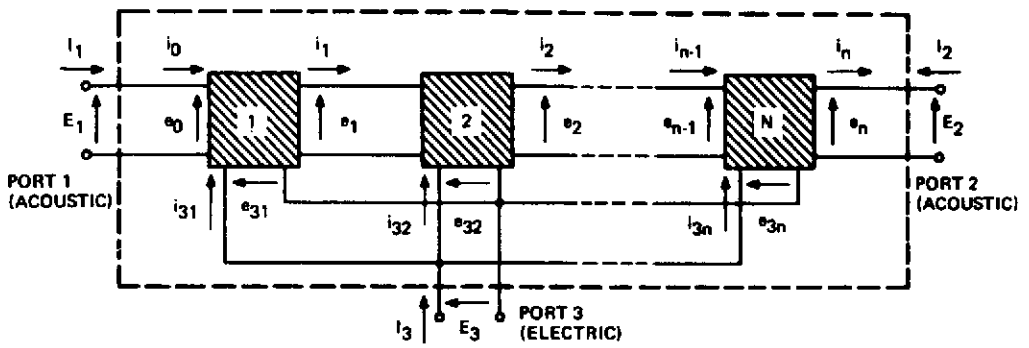

Fig. 24. Transducer equivalent circuit for N periodic sections (acoustically in cascade and electrically in parallel).

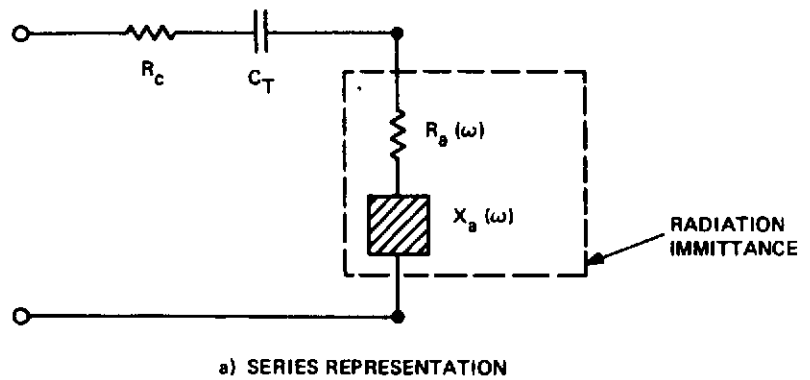

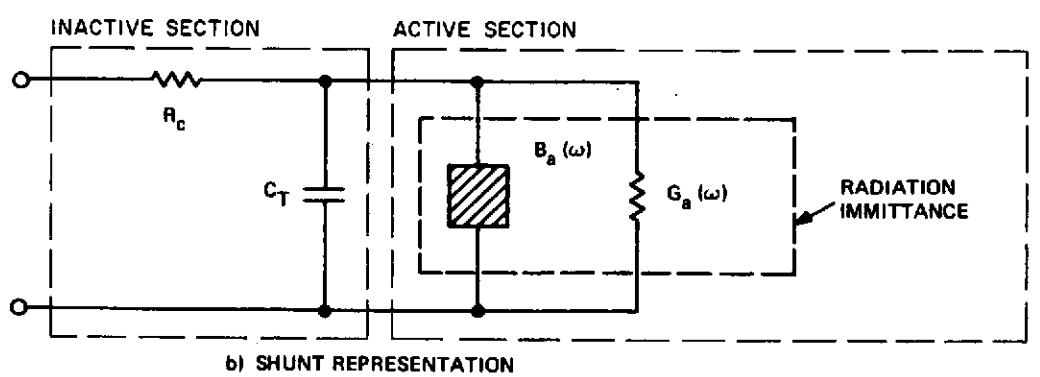

Fig. 25. Equivalent circuits for the interdigital transducer electrical immittance.

```
ARRAY CENTER FREQUENCY IN MHZ = 60

CALCULATION FREQUENCY IN MHZ = 60

CHOOSE K**2 = .0482 FOR LITHIUM NIOBATE, = .00116 FOR ST-QUARTZ
K**2 = .0482

BANDWIDTH IN MHZ = 10

PULSE LENGTH IN MICROSECONDS = 5

RALEIGH WAVE VELOCITY = 3.48E5 CM/SEC FOR LITHIUM NIOBATE
RALEIGH WAVE VELOCITY = 3.16E5 CM/SEC FOR ST-QUARTZ
CHOOSE WAVE VELOCITY = 3.425E5

WIDTH OF FINGER IN MICROINCHES = 500

APERTURE AT CENTER FREQUENCY IN WAVELENGTHS = 15

EFFECTIVE DIELECTRIC CONSTANT = 50 FOR LITHIUM NIOBATE
EFFECTIVE DIELECTRIC CONSTANT = 4 FOR ST-QUARTZ
EFFECTIVE DIELECTRIC CONSTANT = 50

IF YOU WANT TOTAL FINGER CAPACITANCE, CT, TYPE 1
IF YOU WANT CONDUCTANCE, SUSCEPTANCE AND CT, TYPE 2
DESIRED DATA NUMBER = 2

M= 312    N= 287    CSM= .322131    CSN1= .406601

N2=-312   NA= 45   GI= .5378E-03   BI= .9785E-04   F= 64.97
N2=-282   NA= 75   GI= .8876E-03   BI= .1541E-03   F= 64.73
N2=-252   NA= 90   GI= .1052E-02   BI= .1565E-03   F= 64.02
N2=-222   NA= 88   GI= .1016E-02   BI= .1343E-03   F= 63.55
N2=-192   NA= 88   GI= .1003E-02   BI= .1163E-03   F= 63.09
N2=-162   NA= 88   GI= .9901E-03   BI= .9865E-04   F= 62.64
N2=-132   NA= 86   GI= .9546E-03   BI= .7948E-04   F= 62.19
N2=-102   NA= 86   GI= .9388E-03   BI= .5530E-04   F= 61.54
N2= -72   NA= 86   GI= .9276E-03   BI= .4708E-04   F= 61.32
N2= -42   NA= 84   GI= .8898E-03   BI= .2355E-04   F= 60.68
N2= -12   NA= 84   GI= .8729E-03   BI= .2011E-05   F= 60.06
N2=  18   NA= 84   GI= .8594E-03   BI=-.1028E-04   F= 59.70
N2=  48   NA= 82   GI= .8233E-03   BI=-.2652E-04   F= 59.19
N2=  78   NA= 82   GI= .8069E-03   BI=-.4319E-04   F= 58.67
N2= 108   NA= 82   GI= .7904E-03   BI=-.5873E-04   F= 58.17
N2= 138   NA= 80   GI= .7544E-03   BI=-.7246E-04   F= 57.66
N2= 168   NA= 80   GI= .7367E-03   BI=-.8784E-04   F= 57.12
N2= 198   NA= 80   GI= .7187E-03   BI=-.1026E-03   F= 56.59
N2= 228   NA= 78   GI= .6829E-03   BI=-.1137E-03   F= 56.07
N2= 258   NA= 68   GI= .5790E-03   BI=-.1111E-03   F= 55.53
N2= 286   NA= 39   GI= .3232E-03   BI=-.6981E-04   F= 55.02

FOR FREQUENCY =  60.00,  G= .25190  B= .00397

AVERAGE NA= 80.000

M= 312    N= 287    CSM= .322131    CSN1= .406601

TOTAL FINGER CAPACITANCE IN PFD =   107.7187
```

Fig. 26. DRAP output for dispersive transducer.

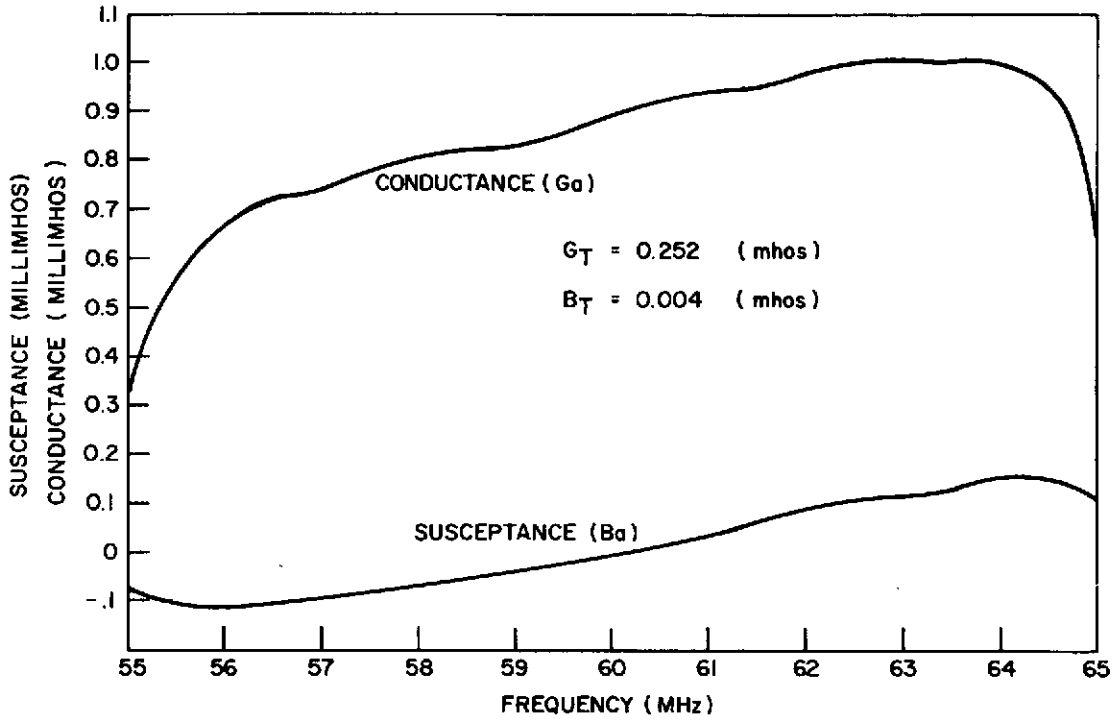

Fig. 27. Dispersive transducer conductance and susceptance per finger pair.

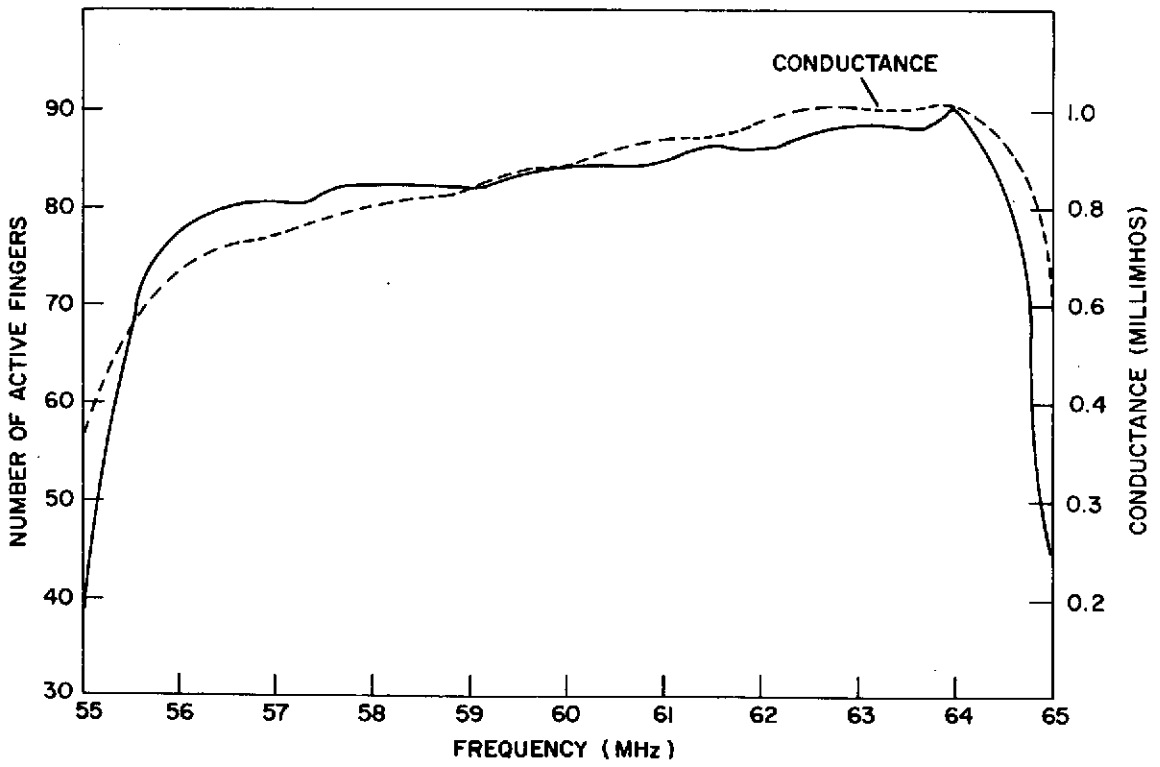

Fig. 28. Variation of active fingers with frequency, with conductance overlay.

All that remains to complete the model in Fig. 25b is to calculate R_c, the ohmic resistance of the IDT structure. R_c is defined below as:

$$R_c = \frac{16\, R_o\, W_n}{3\, N_a(f_o)} \tag{15}$$

where $N_a(f_o)=2\,\pi f \sqrt{\Delta T/\Delta f} = 84$, $R_o = 0.5$ ohms per square, $\Delta T = 5\ \mu s$, $\Delta f = 10$ MHz, and $W_n = 15$. Therefore R_c is approximated at 0.48 ohms midband.

This completes the basic circuit model which now can be used to calculate the transducer efficiency and predict the insertion loss of each transducer. The necessary equation for the transducer efficiency η is:

$$\eta = \frac{4\, R_G\, R_a}{(R_G + R_a + R_c)^2 + (1/wC_T)^2} \tag{16}$$

For $R_G = 50$ ohms, $R_c = .48$ ohms, $R_a = 1/G_T = 4$ ohms and $C_T = 107$ pF, the untuned transducer efficiency is 22%.

If a matching network, a simple series inductor, is used, then $R_G = R_a + R_c$ and $(1/wC_T)^2 \cong 0$, so that the efficiency is:

$$\eta_m = \frac{1}{1 + R_c/R_a} = 89\%. \tag{17}$$

To compute overall insertion loss both power and diffraction efficiencies are used in the equation below [4]:

$$I_L = [(TE)^2\ (DE)]^{-1} \tag{18}$$

with DE = 20%, I_L is 6.3 dB per transducer. Usually 3 dB is added to account for bi-directionality, but long delay lines are highly directional due to wave dispersion. Hence the complete insertion loss for a double transducer configuration would be approximately 12.6 dB, without including parasitic effects of the feed structures, etc.

In summary, the electrical model enables accurate prediction of insertion loss and impedance to evaluate the effect of aperture width, metallization, parasitic capacity, and electrical mismatch.

MATCHED FILTER PULSE COMPRESSION

INTRODUCTION

The matched filter essentially uses the inverse frequency/time response of the pulse expander line to delay one end of the received pulse relative to the other while conserving the energy of the pulse, thus producing at the filter output a narrower pulse of greater amplitude. Figure 29 illustrates the respective frequency/time characteristics of the expanded pulse and the matched filter [11]. As indicated in Figs. 29a, b, and c, the linear time delay characteristic of the filter acts to delay the high frequencies more than the low frequencies, thereby producing a net time compression of the signal while preserving the signal energy. The result is a pulse with greater peak power, but narrower width. The exact steps required to implement pulse compression by surface wave techniques is discussed in the next section.

MATCHED FILTER DESIGN

In the previous section, the theoretical procedure for designing a linear FM expander was presented in some detail. The matched filter design is essentially identical to the expander except for the weighting of the aperture overlap. Since the double dispersive structure only operates in a single time sequence, the FM burst will be inverted in time before being presented to the matched filter. This is illustrated in Fig. 30. As the burst mixes with a 120 MHz ($2f_0$) frequency source, the signal is effectively inverted. After inversion, the signal interacts with the input transducer, causing fingers sensitive to the incoming frequency to launch a wave toward the output from different points along the transducer path. As this wave enters the output array, the fingers extract energy to form the characteristic sidelobes. However, since the full signal comes into "register" with the electrodes, or when each frequency is simultaneously under the proper electrode pair, the extracted energy combines to form the main lobe. Similarly, symmetrical characteristic sidelobes form as the wave propagates out of the transducer. In this way, a sin x/x pattern is produced with a theoretical peak-to-sidelobe ratio of -13.2 dB and with trailing sidelobes falling off at a rate of -4 dB. Figure 31 is a sin x/x compressed pulse obtained from the initial design.

SIDELOBE REDUCTION

As previously noted, the compressed pulse forms a sin x/x pattern with time sidelobes extending on either side of the main lobe. These sidelobes, however, limit the detection capability of the radar by obscuring weaker signals reflected from small or distant targets if simultaneously detected large target pulses contain high sidelobes. Therefore, to extend the radar range and detection, the sidelobes can be reduced by several techniques. The three different approaches for weighting the pulse

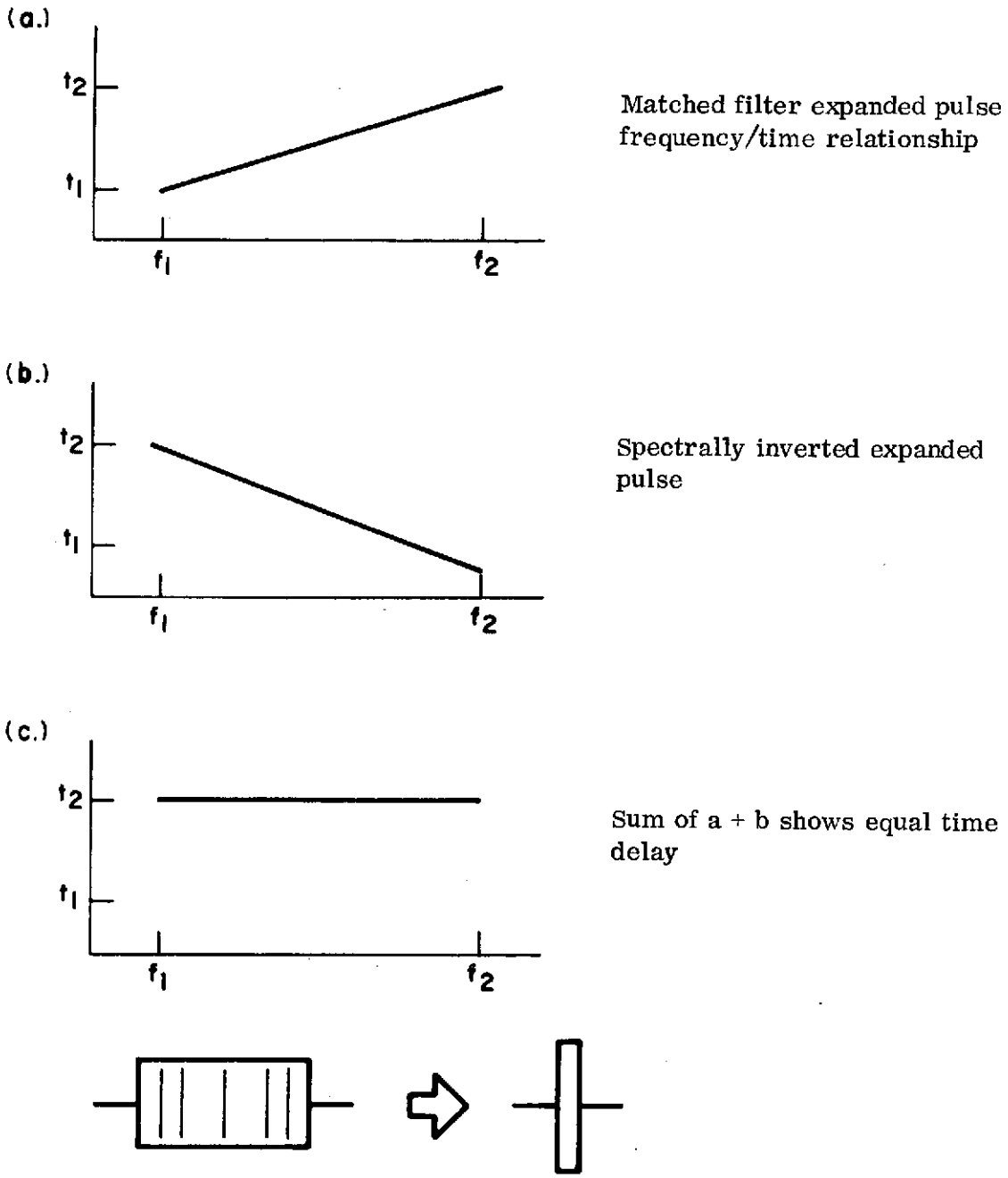

Fig. 29. Frequency/time characteristics of the expanded pulse and the matched filter.

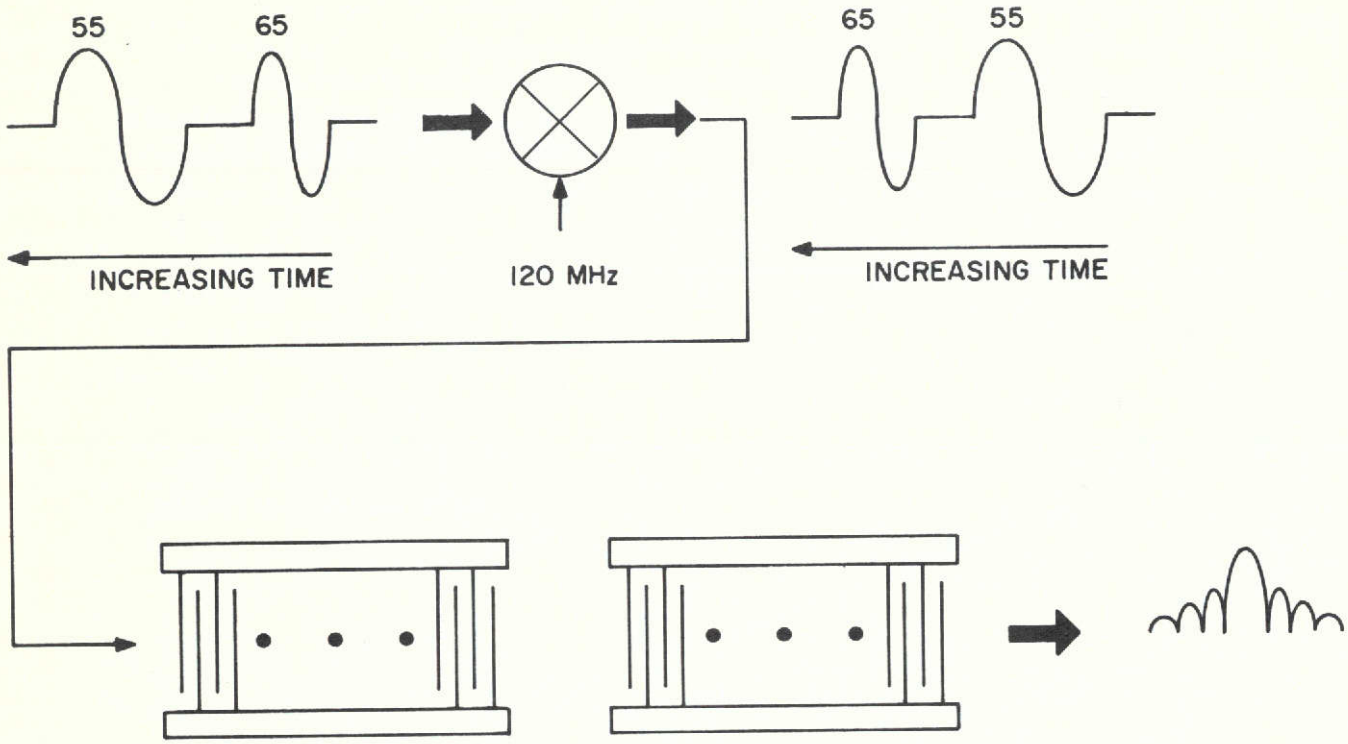

Fig. 30. Schematic representation of frequency inversion and pulse compression.

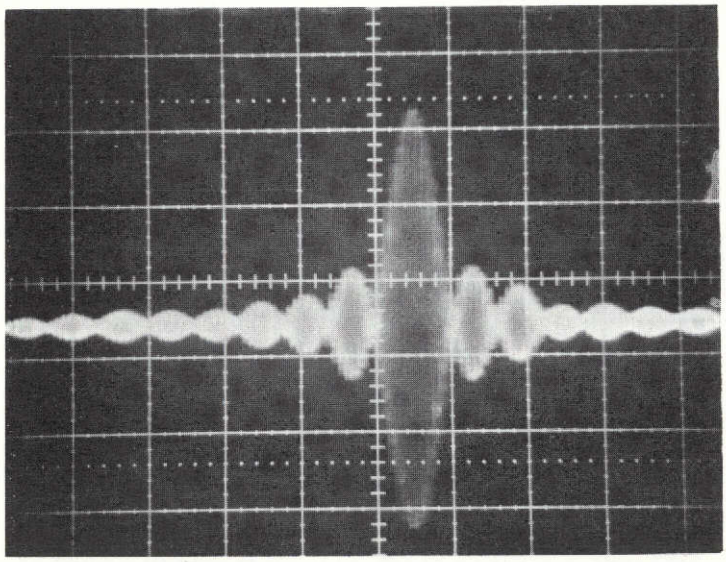

Fig. 31. Compressed pulse obtained from initial design with excellent symmetry.

spectrum are: (1) frequency domain weighting, (2) time domain envelope weighting, or (3) FM pre-distortion. These approaches are summarized in Table VII. Since the main emphasis remains on SAW devices, the most simple and effective techniques to implement are internal time domain weighting or external frequency domain weighting. A separate section is devoted to each approach.

INTERNAL WEIGHTING

Internal weighting involves varying the finger overlap according to a specific weighting function to prevent sidelobes from forming during the compression. Table VIII summarizes the available weighting functions theoretically capable of over 30-dB suppression [2]. The table also contains the effect of each function upon the main lobe width, mismatch loss, and a sidelobe fall-off rate. Since the main lobe width determines the resolution of the radar, any widening due to weighting degrades the radar performance. This effect was taken into account by designing for a higher time-bandwidth product. The mismatch loss reduces the signal-to-noise ratio by causing impedance mismatch due to the varying overlap. Considering the four functions, the Hamming function,

$$H(w) = K + (1-K) \cos^2 \left\{ \pi \left(\frac{f - fo}{\Delta f} \right) \right\}, \tag{19}$$

capable of -42.5 dB sidelobe suppression was selected. The complete design equation, then, for the matched filter is the combination of several design equations. Table IX summarizes the design equations used for the design of the delay line. Each transducer is divided into four sections — two tail sections and two main sections (see Fig. 32).

In summary, this concludes the initial approach to design a high performance surface wave device. Many artwork limitations, however, prohibited subtle adjustments to the equations to equalize phase and velocity performance in the line. The following section discusses these limitations imposed by artwork generation and fabrication of the photomasks.

EXTERNAL WEIGHTING FILTER

Since the FM burst exhibits a narrow bandwidth, SAW technology can be used to fabricate a filter with the Hamming weighting response to suppress undesirable sidelobe levels. Figure 33 is a photograph of the photomask of a bulk wave cancelling filter on $LiBNO_3$. The filter was designed to fit a Hamming weighted response with a 6-MHz bandwidth at the -3 dB points. To implement a SAW filter design, a Fast Fourier Transform (FFT) program using a modified cosine squared function approximates the desired frequency response. Then by taking the transform of this response:

$$H(t) = \frac{1}{2\pi} \int_{-\infty}^{\infty} k(w)\, e^{-jwt}\, dw \tag{20}$$

TABLE VII — TECHNIQUES FOR THE SUPPRESSION OF THE TIME SIDELOBES OF A COMPRESSED FM PULSE

Technique	System Effects
1. Frequency Shaping of the Receiver Bandpass	A very common technique, with less than -40-dB sidelobes possible. Has good doppler characteristics.
2. Delay Line Cancellation (Transversal Filtering)	This technique requires isolation, as well as carrier phase control at each tap position. Reduction of sidelobes to about -30 dB, with a 25-percent increase in compressed pulse width is possible. Synthesized at IF, this approach is sensitive to shifts in frequency.
3. FM Predistortion	This is a reasonably common technique for reducing sidelobes through control of the signal spectrum, and is theoretically capable of -40 dB. Predistortion exhibits good doppler characteristics.

TABLE VIII — WEIGHTING FUNCTION DATA

Weighting Function	Peak Sidelobe Level (dB)	Pulse Widening	Mismatch Loss (dB)	Far Sidelobe Fall-Off Rate
Dolph-Chebyshev	-40	1.35	-	1
Taylor (n = 6)	-40	1.41	-1.2	1/t
$k + (1 - k) \cos^n$				
Hamming:	-42.8	1.47	-1.34	1/t
(k = 0.08, n = 2)				
Cosine-squared:	-32.2	1.62	-1.76	$1/t^3$
(k = 0, n = 2)				

TABLE IX — SUMMARY OF DESIGN EQUATIONS

Sect.	Frequency (MHz)	Time* (μs)	Transmitter**		Receiver	
			TX Eqs.	TY Eqs.	RX Eqs.	RY Eqs.
1	54 -55	0 - 0.5	4 • 5	10 • 12	4 • 5	11 • 12 • 19
2	55 - 60	0.5 - 3		10		11 • 19
3	60 - 65	3 - 5.5		11		10 • 19
4	65 - 66	5.5 - 6		11 • 12		10 • 12 • 19

Notes: *Time per transducer.
**X is finger position, Y is apodization.

the impulse response of the filter is determined. From the impulse function, a finger overlap pattern is generated to produce a photomask which produces filters using the techniques outlined in the section on fabrication. In addition to the conventional design approach, a scheme to eliminate bulk waves by phase cancellation was implemented to improve the filter sidelobes. The technique utilizes a unique finger pattern incorporating a floating finger to phase reverse the signal at midpoint. In this way, half the surface and bulk waves are launched 180° out of phase. A thin metal film covering half the beamwidth shifts the surface wave 180° to place the wavefronts in phase to constructively add, while the bulk waves remain out of phase and cancel out. The scheme worked but produced an unexpected triple transit response which eventually degraded the performance of the system. This was discussed in detail in the performance evaluation section.

DESIGN LIMITATIONS

Although the previous sections detailed the complete design approach, fabrication equipment limitations required some compromises in the transducer geometry and waveform modulation. Basically, the mechanical round off of .2-mil least step on the Gerber artwork generators produced many design tradeoffs. The 10 -μs line corresponds to a 1 X length of 1.8 inches, while the maximum photographic plate size is 30 x 40 inches. Consequently, this limits a maximum pattern size to a 20X magnification. Since this 20X pattern must be reduced by a 20X lens which is accurate only within a 16-inch square, slight pattern distortion of each end of the transducer will occur. To balance this distortion the double dispersive geometry was utilized.

Fig. 32. Design sections of the SAW delay line.

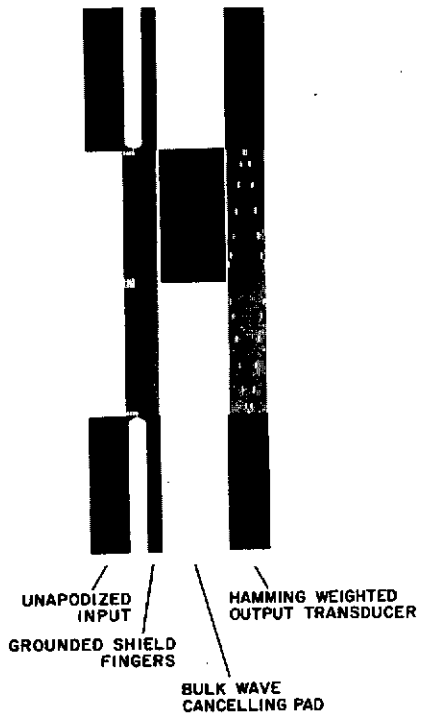

Fig. 33. Bulk wave cancelling SAW weighting filter photomask.

The second design tradeoff transformed the linear FM equation into a stepwise linear FM approximation to meet the .2-mil mechanical round off specification of the Gerber artwork generator. As indicated in Fig. 34, the number of finger pairs per frequency step decreases as the frequency decreases. This also appears in Fig. 35 with the frequency step changing as the spacing changes. This situation completely eliminates the ability to adjust for velocity changes within the array; therefore, phase error will accumulate and raise the main sidelobes.

Another degradation occurs when the stepwise linear pulse is frequency inverted since the frequency-time relationship in the inverted mode is not the same. In other words, when the expanded pulse is generated, the high frequency end has a .6-MHz least step which decreases in time to a .4-MHz least step at the low frequency end. When the inversion is performed, the .4-MHz step translates to the high frequency end, and the .6-MHz step translates to the low frequency end, thereby decorrelating the frequency time relationship. Consequently, the inverted pulse frequencies do not respond to the finger pair separations, since the line is not symmetrical as in a linear FM line. It was determined that approximately 15% of the finger pairs will be inactive in the compression mode. Table X shows the frequency mismatch with every other frequency step indicated. The overall effect of this situation will be to decrease the time bandwidth product, thereby increasing the pulse width and raising the time sidelobes.

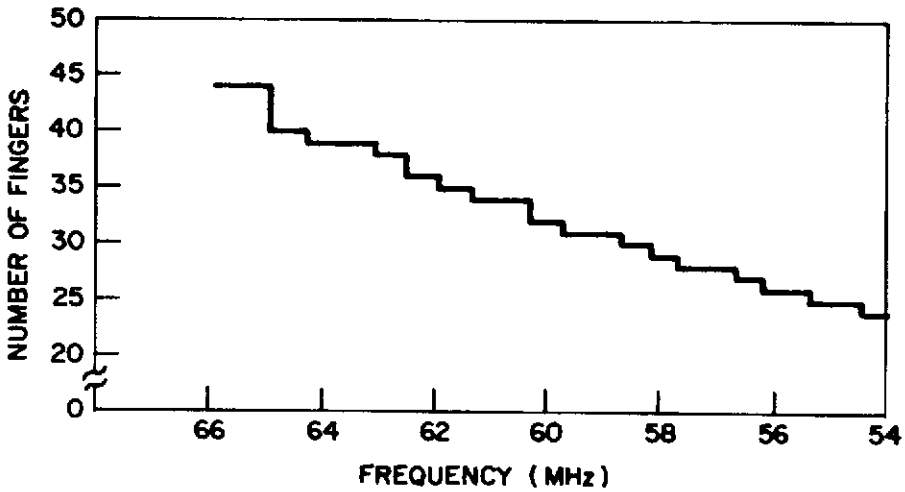

Fig. 34. Active finger variation across the specified bandwidth.

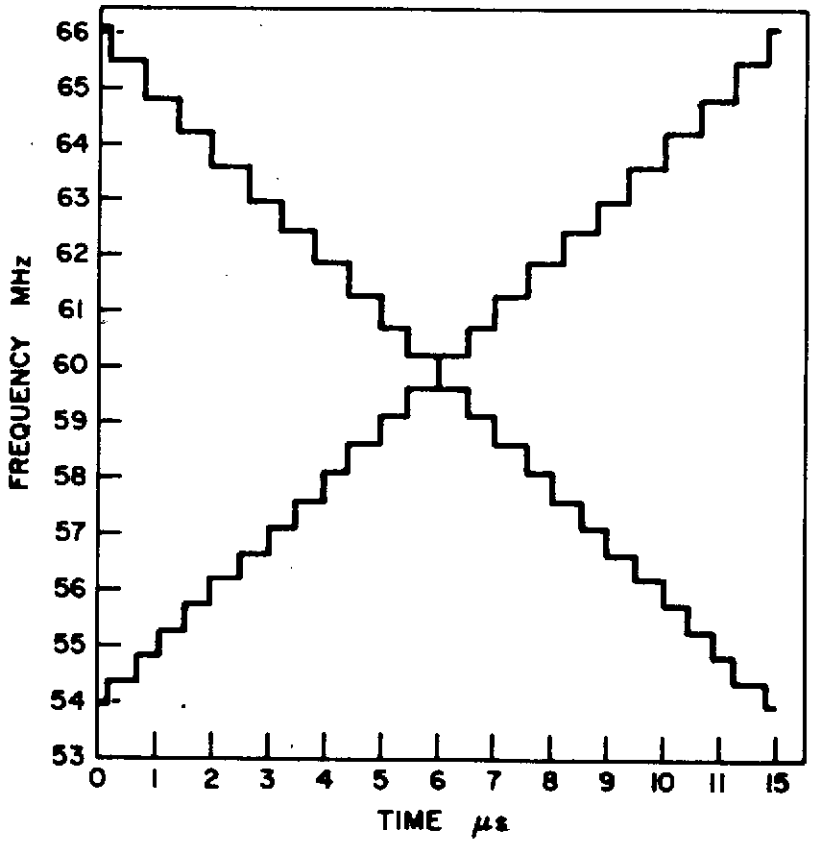

Fig. 35. Theoretical frequency-time characteristics of the FM line.

TABLE X - FREQUENCY-TIME MATCHING OF INVERTED AND NON-INVERTED EXPANDED PULSE (Every other step is included)

Design (MHz)	Inverted (MHz)	Matched (MHz)
65.5	54.5	54.4
64.2	55.8	55.3
63.0	57.0	56.2
62.5	57.5	56.7
61.3	58.7	57.7
60.2	59.8	58.7
59.2	60.8	59.7
58.2	61.8	60.8
57.2	62.8	61.9
56.2	63.8	63.0
55.3	64.7	64.2
54.4	65.6	65.5

Furthermore, the original intention was to produce two separate lines, one with flat amplitude response for transmission and the other with Hamming weighting for reception. It was finally decided to utilize only the Hamming weighted line and eliminate the weighting function by amplification and limiting. This resulted in a slightly narrower bandwidth and shorter pulse length due to the extremely weighted transducer ends and diffraction losses at small aperture overlaps. However, by cascading weighting filters, the narrow bandwidth can be accommodated.

The next section discusses the fabrication techniques and principles.

FABRICATION

Implementing the design equations previously discussed requires extensive use of the Spectra 70 computer. Figure 36 illustrates the steps involved to create a tape to drive the Gerber artwork plotters. Briefly, the design procedure is an iterative process which calculates electrode spacing and finger lengths for each interdigital pair. Step 1 is the design of the transducers and the creation of specially formatted tape providing incremental data to the Gerber program. Step 2 converts the Gerber instructions from card to tape, then Step 3 merges the incremental data with the pen instructions producing an executable program called "Monitor." Step 4 converts the

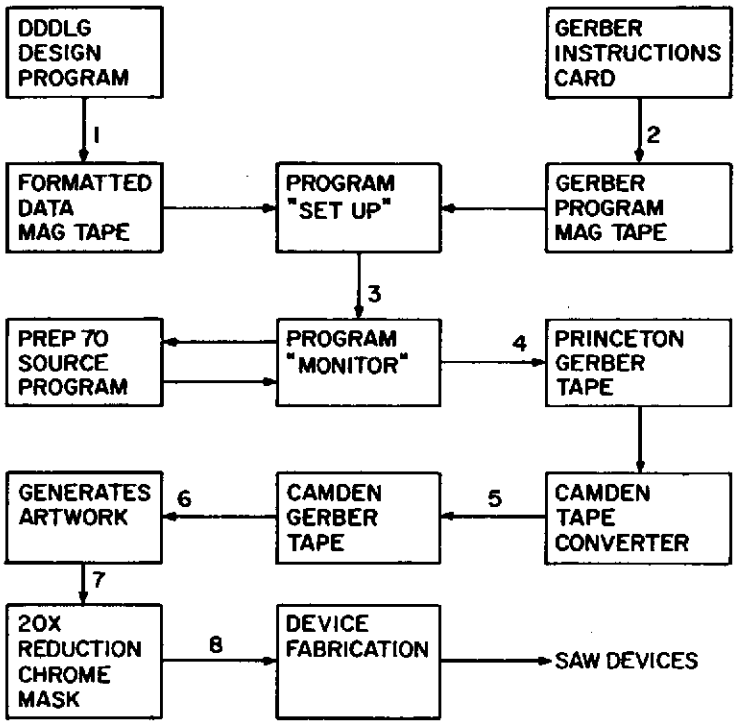

Fig. 36. Flow chart for SAW devices from design to fabrication.

instructions to step-by-step commands for the plotter creating a tape specified as "Gerber tape." These instructions, however, apply only to the Gerber 1032 model; hence, Step 5 is required to convert the commands to drive the Gerber 632 which is based in the Camden facility. After the artwork is drawn on 30-inch x 40-inch glass, the 20X pattern is optically reduced to 1X onto a 2 1/2-inch x 2 1/2-inch x 0.060-inch glass glass plate. The photomask transfers the finger pattern onto the $LiBNO_3$ crystals with standard photolithographic techniques. In brief, the actual processing steps shown in Fig. 37 are:

1. Procure 2.5-inch x .375-inch x 0.040-inch Y-Z cut $LiBNO_3$ crystals oriented 6 min to the Z-axis,
2. R-F sputter a 1500-Å aluminum film onto the substrate surface,
3. Apply Shipley positive photoresist to the aluminum film,
4. Align the photomask to the edge of the crystal,
5. Expose the photoresist to a collimated light source,
6. Etch the unexposed photoresist leaving a finger pattern,
7. Etch the exposed aluminum and remove photoresist leaving the metalized pattern.

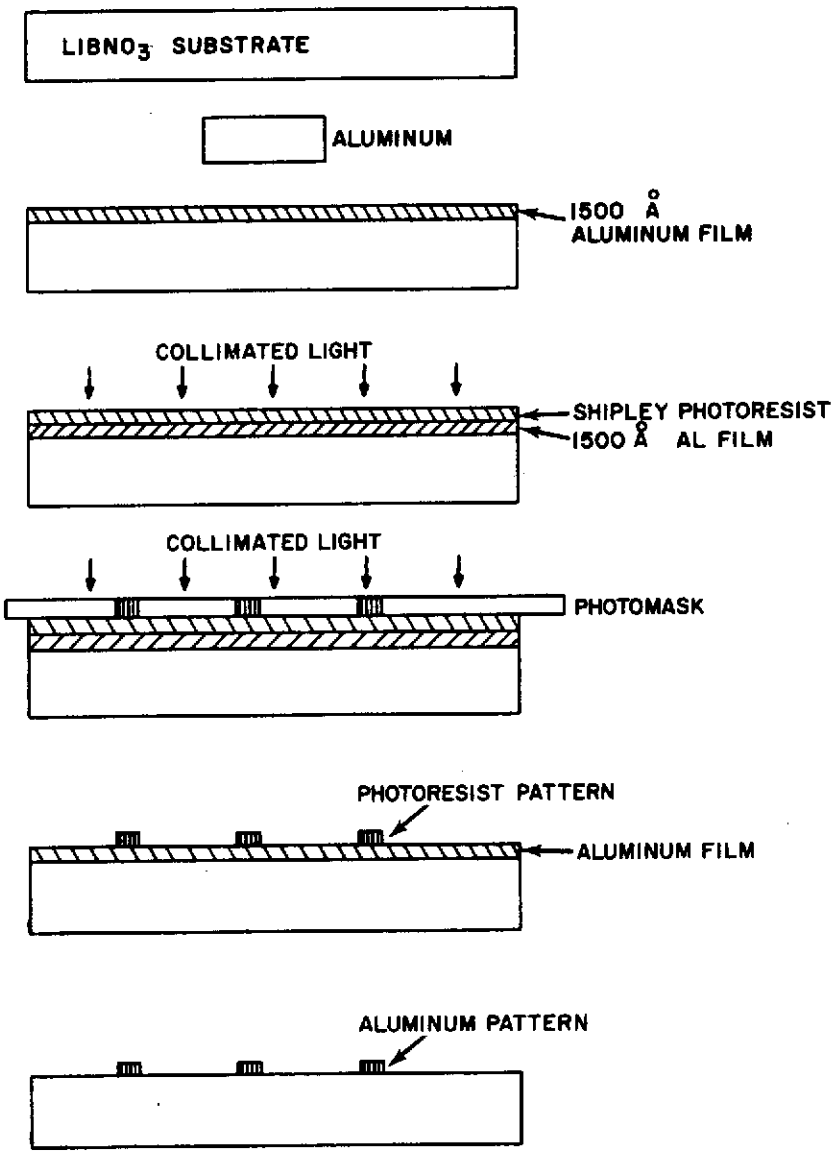

Fig. 37. Schematic illustration of the principles of planar fabrication technique.

REFERENCES

(1) Szabo, T. A. and Slobonik, A. J., Jr., "The Effect of Diffraction on the Design of Acoustic Surface Wave Devices," IEEE Transactions on Sonics and Ultrasonics, Vol. SU-20, No. 3, July 1973.

(2) Cook, C. E. and Bernfeld, M., Radar Signals An Introduction to Theory and Design, Academic Press, New York, 1967.

(3) Sittig, E. K. and Cocquin, G. A., "Filters and Dispersive Delay Lines Using Repeatively Mismatch Ultrasonic Transmission Lines," IEEE Transactions on Sonics and Ultrasonics, Vol. SU-15, April 1968.

(4) Gerald, H. M. and Smith, W. R., et al, "The Design and Application of Highly Dispersive Acoustic Surface Wave Filters," IEEE Transactions on Sonics and Ultrasonics, Vol. SU-20, No. 2, April 1973.

(5) Smith, W. R., Gerald, G. M., Collins, J. H., Reeder, T. M. and Shaw, H. J., "Design of Surface Wave Delay Lines with Interdigital Transducers," IEEE Transactions on Microwave Theory and Tech., Vol. MTT-17, No. 11, Nov. 1969, p. 866.

(6) Grasse, G. L., Private Communication.

(7) Smith, W. R., Gerald, H. M., et al, "Analysis and Design of Dispersive Interdigital Surface Wave Transducers," IEEE Transactions on Microwave Theory and Techniques, Vol. MTT-20, No. 7, July 1972.

(8) Williamson, R. C., "Measurement of the Propagation Characteristics of Surface and Bulk Waves in $LiBNO_3$," Presented at the 1972 IEEE Ultrasonics Symposium, Oct. 4-7, 1972.

(9) Tancrell, R. H. and Williamson, R. C., "Wavefront Distortion of Acoustic Surface Waves from a Produced Interdigital Transducer," Appl. Phys. LETT., Vol. 19, pp. 456-459, Dec. 1971.

(10) Smith, W. R., et al, "Analysis of Interdigital Surface Wave Transducers by the Use of an Equivalent Circuit Model," IEEE Transactions on Microwave Theory and Techniques, Vol. MTT-17, No. 11, Nov. 1969, p. 857.

(11) Mason, W. P., Electromechanical Transducers and Wave Filters, Second Edition, Princeton, N. J.: Van Nostrand, 1948, pp. 253-255.

(12) Herring, F. G., et al, "High Performance Surface Wave Pulse Compression," Presented in IEEE Ultrasonics Symposium, 1973.

DISTRIBUTION LIST

NASA Lyndon B. Johnson Space Center:	No. of Copies
Advanced System Procurement Section Attn: Contracting Officer, Mail Code BC76(81) Houston, TX 77058	1
Technical Library Branch Attn: Retha Shirkey, Mail Code JM6 Houston, TX 77058	4
Management Services Division Attn: John T. Wheeler, Mail Code JM7 Houston, TX 77058	1
Tracking Techniques Branch Attn: EE6/R. C. Kelly Houston, TX 77058	10